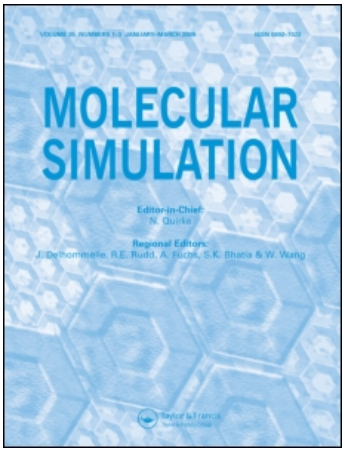

Molecular Simulation
Publication details, including instructions for authors and subscription information:
http://www.informaworld.com/smpp/title~content=t713644482

GCEMC Simulations of "Swiss Cheese" Ion Exchange Membranes in Dilute Solutions of Primitive Model 1:1 Electrolytes with Different Sizes of Ions or 2:1 Electrolytes with Different Bjerrum Parameters

Torben Smith Sørensen[a]; Sergio Roberto Rivera[ab]
[a] Physical Chemistry, Modelling and Thermodynamics, Vanløse, Denmark [b] Facultad de Físico-Química, Universidad de Concepción, Chile

To cite this Article Sørensen, Torben Smith and Rivera, Sergio Roberto(1995) 'GCEMC Simulations of "Swiss Cheese" Ion Exchange Membranes in Dilute Solutions of Primitive Model 1:1 Electrolytes with Different Sizes of Ions or 2:1 Electrolytes with Different Bjerrum Parameters', Molecular Simulation, 15: 2, 79 — 122
To link to this Article: DOI: 10.1080/08927029508022332
URL: http://dx.doi.org/10.1080/08927029508022332

Molecular Simulation, 1995, Vol. 15, pp. 79–122
Reprints available directly from the publisher
Photocopying permitted by license only

GCEMC SIMULATIONS OF "SWISS CHEESE" ION EXCHANGE MEMBRANES IN DILUTE SOLUTIONS OF PRIMITIVE MODEL 1:1 ELECTROLYTES WITH DIFFERENT SIZES OF IONS OR 2:1 ELECTROLYTES WITH DIFFERENT BJERRUM PARAMETERS

TORBEN SMITH SØRENSEN* and SERGIO ROBERTO RIVERA¶

Physical Chemistry, Modelling and Thermodynamics, Danmarks Tekniske Højskole Nørager Plads 3, DK 2720 Vanløse, Denmark

(Received December 7, 1994, accepted March 1995)

Monte Carlo simulations using a Markov process corresponding to a (generalized) Grand Canonical Ensemble have been performed for a number of spherical micropores in equilibrium with dilute external bulk solutions of primitive model electrolytes. Dilute solutions of 1:1 electrolytes with a Bjerrum parameter $B = 1.546$ with cations three times larger than the anions have been simulated. Also, dilute solutions of 2:1 electrolytes with ions of equal size and reduced Bjerrum parameters $B_r = 1.546$ and 3 have been simulated. The pores are primitive pores with hard walls and the same dielectric permittivity in the wall and in the pore solution. They range from a pore radius = 5 times the mean ionic diameter to 35 times this diameter, and they carry a fixed charge equal to + 5, 0 and − 5 elementary charges. The fixed charge is modelled as smoothly distributed on the pore-wall interface. In addition to the electric potential of the interfacial charge and the electric potential of the spherical double layer, a potential Δ between the pore solution and the bulk solution may be deliberately added. For single pores we may take $\Delta = 0$, but then the pore is generally not electroneutral. In a "Swiss cheese" membrane with a lot of (equally sized) pores, the membrane phase has to approach electroneutrality for growing size of the phase. This is approximated by means of a membrane generated potential Δ in each pore (from the electrostatic interactions with the other pores). The potential Δ so chosen to obtain electroneutrality is the GCEMC Donnan potential. These non-ideal Donnan potentials are compared to the ideal values (with activity coefficients equal to zero). From the mean occupation numbers of cations and anions in the pores, the average pore values of the mean ionic and the single ionic activity coefficients of the ions are calculated. These are very dependent on pore sizes and on the potential in the pore. The excess energy and the electrostatic Helmholtz free energy of the ions in the pores are also simulated directly. The electrostatic entropy is found as the difference.

KEY WORDS: Spherical charged micropores, primitive model electrolytes, spontaneous electrification, Donnan potentials, pore activity coefficients, excess thermodynamic quantities, Grand Canonical Ensemble Monte Carlo, ion exchange membranes.

INTRODUCTION

A small number of statistical mechanical studies of ions and particles in micropores have been performed. For example, Zhou and Stell have made an integral equation approach (HNC, PY and BBGKY) to the problem of hard spheres inside spherical and

* To whom all correspondence should be sent.
¶ Address after February 1, 1995: Facultad de Físico-Química, Universidad de Concepción, Chile.

slit pores [1] and to the problem of ion- and potential distributions in water-in-oil microemulsions [2]. Pair correlation functions for hard sphere fluids in narrow slits have been studied by Kjellander and Sarman [3] from the point of view of the anisotropic PY approximation in order to understand the mechanism of oscillatory solvation forces.

Canonical Ensemble Monte Carlo (CEMC) was used by Zara et al. [14] to study mixed valency counterions between charged plane walls, and the simulations were compared to the solution to the Poisson–Boltzmann equation. Vlachy and Haymet [5,6] have performed Grand Canonical Ensemble Monte Carlo (GCEMC) simulations of 1:1 and 2:2 electrolytes in cylindrical micropores. Common to the studies [4–6] is the fact, that electroneutrality is always assumed in the simulation cell. Especially in the case of GCEMC the spirit of the method is contradicted to some degree by this assumption, since the occupation number of each ion is determined as a fluctuating quantity by the fixed electrochemical potentials in the external solution, and there is no guarantee of electroneutrality in small systems.

Sørensen and Sloth [7,8] have performed GCEMC simulations of ions inside spherical micropores with continuously distributed surface charge and with the same dielectric permittivity in the pore and in the hard wall. Such pores are called "primitive pores'. The electrolytes were primitive model electrolytes. Occupation numbers and one particle distribution functions $G_i(r)$ ($i = +$ and $-$) of the ions were simulated. The electric potential distributions were calculated and compared to various solutions to the Poisson–Boltzmann equation in dilute and in moderately concentrated systems. In reference [7], a few Donnan potentials were also found. This is the additional electric potential (Δ) which has to be applied to the pore in order to ensure electroneutrality. In a "Swiss cheese" membrane with many (identical) spherical pores, this potential is stemming from the very slight deviation from electroneutrality of the other pores in a phase of finite size. See the discussion in reference [7], pp 585–587.

After the original works of Donnan [9,10], the Donnan potential has been treated previously to the GCEMC study in reference [7] from the point of view of McMillan–Mayer method and Debye–Hückel theory (point ions) by Hill [11], MSA theory by Stell and Joslin [12] and other integral equation approaches, too, by Zhou and Stell [13].

In reference [7], the GCEMC occupation numbers and the GCEMC Donnan potentials were also used for the calculation of the average mean ionic and single ionic activity coefficients in the pore. Furthermore the mean ionic one particle distribution functions $G_{\pm}(r)$ and the electric double layer potential distributions $\Delta\Psi(r)$ in the pore were calculated in references [7,8]. The $G_{\pm}(r)$ seems to be determined by two conflicting influences: A repulsion from the wall due to the breaking of the symmetry of the ionic atmosphere (scale of the order of the Debye length), and an "effective hard sphere/hard wall attraction" (scale of the mean diameter of the ions a). The electric potential distributions may be calculated from a "generalized Debye–Hückel theory" in the case of dilute external salt solutions, see reference [7].

In two previous papers [14,15], the present authors have continued these studies using much longer simulation runs and using a lot of different pore radii and pore charges. In reference [14], pores with radii from 1 to 35 ionic diameters and carrying surface charges from 0 to 10 elementary charges were studied. The pores were in equilibrium with restricted primitive model electrolytes (RPM ~ ionic diameters equal)

with Bjerrum parameters (B) equal to 1.546 (large univalent ions at 25°C in water), 1.681, 2.0 (normal hydrated ions) and 6.8116 (2:2 electrolytes or 1:1 electrolytes at low dielectric permittivity). The electrolyte concentrations were from very dilute to moderately concentrated.

When the potential Δ is put to zero, the pore acquires a net charge of the same sign as the fixed charge, which is called the spontaneous electrification $\langle EL \rangle$, which is only zero for RPM electrolytes and non-charged pores. In other cases, for each surface charge in the pore $\langle EL \rangle$ is a function of $\tau\kappa a$ only without regard to B and the concentration along (κa). Here, τ is the radius of the accessible part of the pore $= (R/a) - 0.5$, κ is the inverse Debye length and a is the common ionic diameter. Only in the case of $B = 6.8116$ and small pore radius and/or small concentration, deviations from the pattern were seen due to contact adsorption of counterions to the fixed charge, see reference [14], Figs. 1 and 2. The Donnan potentials are found as the values of Δ for which $\langle EL \rangle = 0$, see reference [14], Figs. 3–5. The deviations from the ideal Donnan potential were found to be only few percent for dilute electrolyte. For higher concentrations (where the Donnan potentials themselves are smaller), the deviations may be up to 25%. Smaller pores (with higher Donnan potentials) exhibit smaller deviations from the ideal values. The ion–ion interactions are weak, since the ions are often alone in the pores.

The geometric mean occupation number $\langle N_{\pm} \rangle$ seems only to be a function of the total applied potential (TAP) in the pore, i.e., Δ added to the potential created by the fixed pore charge, when the radius of the pore is fixed, see reference [14], Figs. 8a–8c. There is a general increase in $\langle N_{\pm} \rangle$ with TAP– most strongly for small pores and dilute solutions – which we have called electrosorption. This corresponds to a decrease in the average mean ionic activity coefficient in the pore, $y_{\pm}$ (pore), with TAP, see reference [14], Fig. 9. The average single ion activity coefficients in the pore may also be found at any Δ, pore charge and pore radius. For small pores, these are very sensitive to variations in the components of the total applied potential.

The internal energy ($\langle U \rangle$) of the ions in the pores was also sampled. In chargeless pores, the quantity $U/\{kT\langle N_{\text{total}} \rangle\}$ divided by the values from *canonical* ensemble MC, $E_{\text{ex}}(\infty)/NkT$, extrapolated to the thermodynamic limit ($N \to \infty$, concentration constant), may be plotted vs $1/(\tau\kappa a)$ as monotonously decreasing curves. (The internal energy is truncated for smaller pores or smaller concentrations, where there are only few ions in the pore). The curves extrapolate nicely to unity for $1/(\tau\kappa a) \to 0$ (bulk solution), see reference [14], Fig. 13. How to extrapolate canonical ensemble averages of thermodynamic quantities to the thermodynamic limit is a science in itself, see references [16–21].

In reference [14], Appendix B, an analytical theory for minimal, spherical pores was derived. A minimal pore is a pore with room for maximum one ion. This theory is in certain respects a limiting model for small pore size for the GCEMC calculations, but in other respects, there are marked differences. Especially, the Debye length has no significance in the minimal pore model, since there can be no ion–ion interactions in the pore. Also, a Donnan potential exists only in special cases.

In reference [15], two moderately concentrated RPM electrolytes ($\kappa a \approx 0.9$ and 1.4) with $B = 1.681$ were investigated. The surface charges ranged from 0 to 10 elementary units and the pore radii from 2 to 9 ionic diameters. The focus was on the charge and

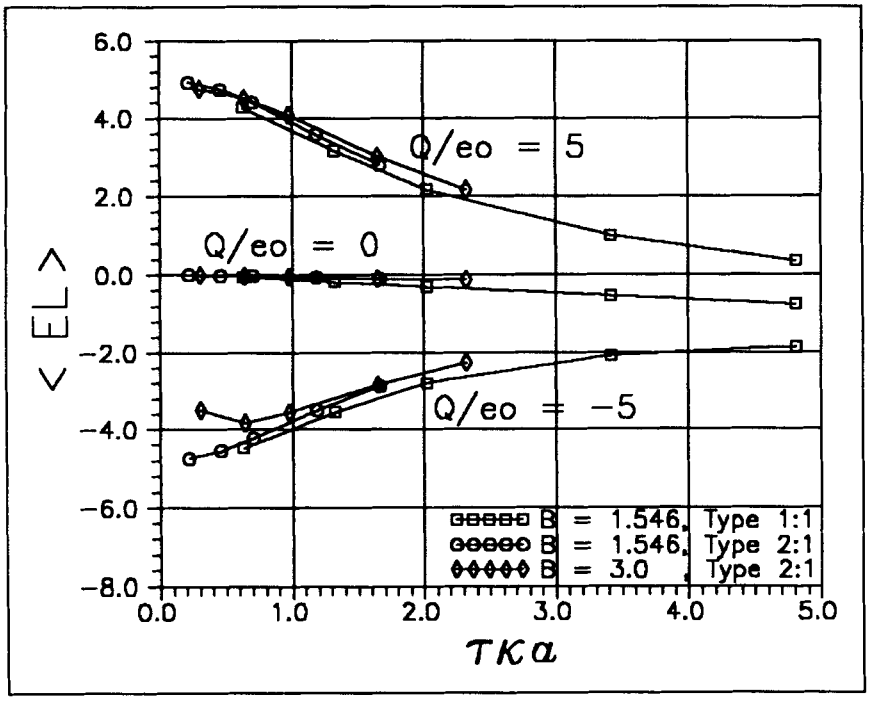

Figure 1 The spontaneous electrification of single pores in contact with dilute primitive model electrolytes. The three electrolytes are the following: (1) A 1:1 electrolyte with the cation three times as large as the anion, Bjerrum parameter $B = 1.546$ and dimensionless salt density $\rho_s^* = 0.0005$ (squares). (2) A 2:1 electrolyte with the doubly charged cation and the singly charged anion of the same size, reduced Bjerrum parameter $B_r = 1.546$ and dimensionless salt density $\rho_s^* = 0.00002$ (circles). (3) A similar 2:1 electrolyte with $B_r = 3$ and $\rho_s^* = 0.00002$ (diamonds). The ordinate is the mean available radius of the pore τa divided by the inverse Debye length in the bulk solution (κ^{-1}). Small values of $\tau\kappa a$ mean either small pores or small concentrations. In this limit $\langle EL \rangle$ tends to Q/e_o except for the 2:1 electrolyte with $B_r = 3$ and $Q/e_o = -5$ due to contact adsorption of the doubly charged cations to the wall charge. This lowers the efficient charge in small pores. Notice the negative spontaneous electrification in large pores without charge. The reason is either predominance of small cations near the wall (1:1) or higher repulsion of the doubly charged cations from the wall (2:1) due to the breaking of the ionic cloud symmetry. The curves for $Q/e_o = \pm 5$ are symmetric around the curve for $Q/e_o = 0$, but not around $\langle EL \rangle = 0$.

potential distributions in the spherical, electric double layer, and on the $G_{\pm}(r)$. The latter showed the above-mentioned competition between "asymmetric ionic cloud repulsion" and "hard sphere/hard wall attraction". There is a tendency of electrodesorption, i.e., decreasing $\langle N_{\pm} \rangle$ with increasing TAP. This is in contrast to the electrosorption in dilute systems. The electric potential distribution may often be fit by only one eigenfunction of the Laplace operator like in the Debye–Hückel treatment, but with a fitted λa instead of κa. In some cases two eigenfunctions were necessary, one with $\lambda a \approx \kappa a$ and one with a purely imaginary λ, see Table 3 in reference [15]. For the larger pores it was extremely difficult to obtain correct potentials near the centre of the pore. Excessive runs amounting to more than 500 millions of configurations have to be

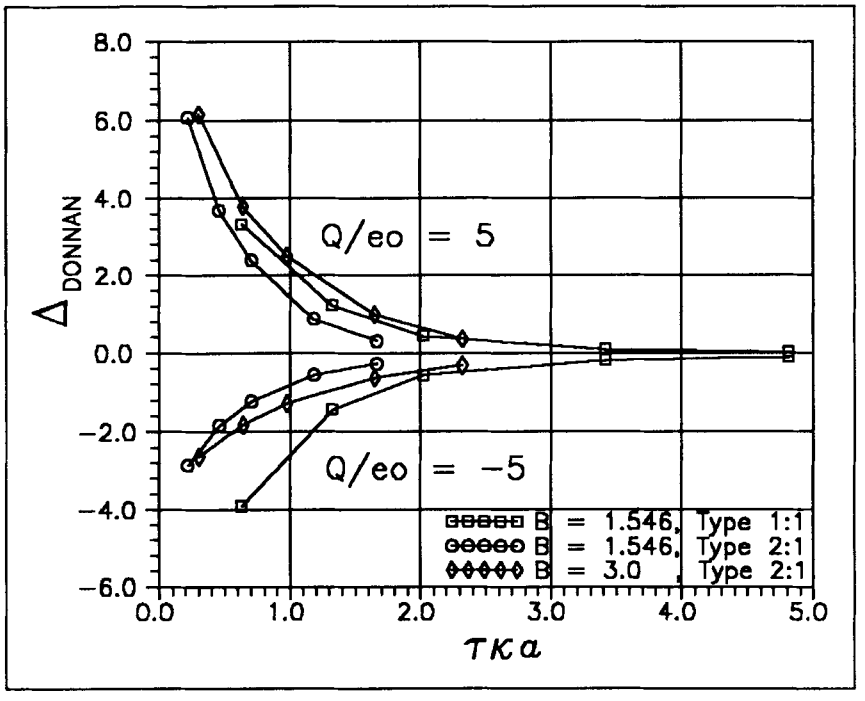

Figure 2 The dimensionless Donnan potentials for the same three electrolytes as in Fig. 1. The Donnan potential is found as the potential $(-\Delta)$, which should be applied to the external, bulk solution in order to obtain $\langle EL \rangle = 0$ in the GCEMC simulation. The Donnan potentials for $Q/e_0 = 5$ and $Q/e_0 = -5$ are unsymmetrical around the line of zero potential.

made in order to bring down the "noise" and also the systematical errors in the very small charge densities in the middle of the pores. (Small systematic errors are due to the arbitrary initial conditions of the Markov chain, for example, starting with an empty pore).

All the above-mentioned GCEMC simulations have been performed with restricted primitive model electrolytes (same absolute value of the valence and same size of the ions). In the present paper we concentrate on a dilute 1:1 electrolyte with a cation three times greater than the anion. Furthermore, two dilute 2:1 electrolytes are studied, where the doubly charged cation and the singly charged anion have the same size. The size/charge asymmetry has, for example, the consequence that simulations with surface charges $\pm Q$ are not identical. The present paper will be an analogue of reference [14], since we shall postpone the treatment of the ion and potential distributions to a later paper. However, the methods for finding single ion activity coefficients have to be generalized.

The farsighted perspective in all these studies is, for example, to be able to understand better certain types of membranes. Many artificial membanes for desalination are based on a two-phase structure: One phase (the continuous) is rich in polymer, and the

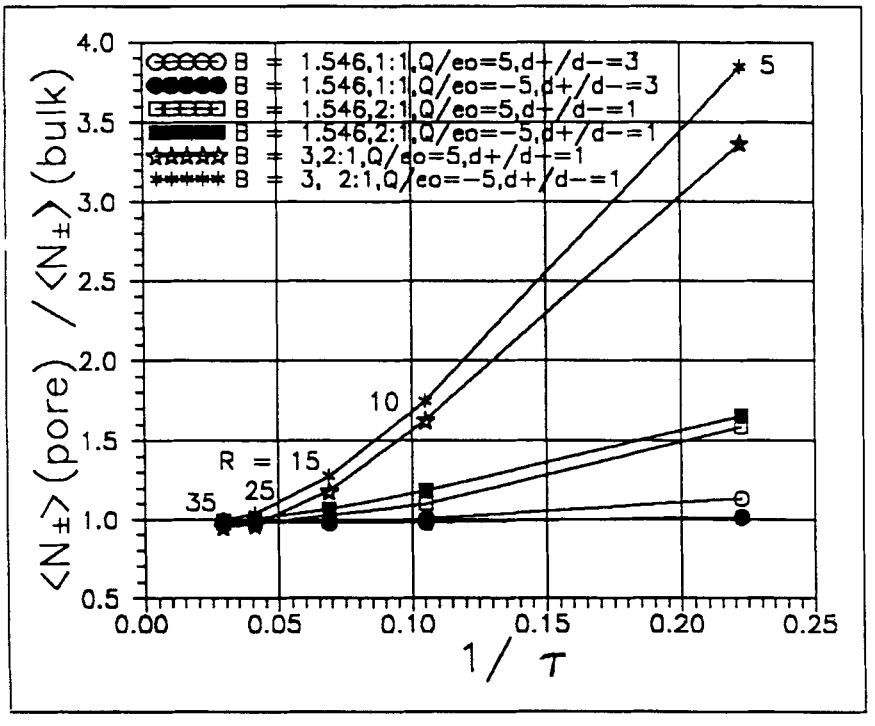

Figure 3a The mean occupation numbers at pore electroneutrality in the pore relative to the mean occupation numbers in the bulk for the three electrolytes (type, B_r, ρ_s^*, d): (1:1, 1.546, 0.0005, 3), $Q/e_o = 5$ open circles, $Q/e_o = -5$ black circles. (2:1, 1.546, 0.00002, 1), $Q/e_o = 5$ open squares, $Q/e_o = -5$ black squares. (2:1, 3, 0.00002, 1), $Q/e_o = 5$ open stars, $Q/e_o = -5$ black stars. The abscissa is the inverse mean available dimensionless pore radius ($1/\tau$). The R-values indicated are the dimensionless ones (R/a). There is a strong "electrosorption" of the 2:1 electrolyte with $B_r = 3$ in small charged pores.

other (the discrete phase) contains more water. The water rich phase has an alveolar structure, since it is formed by droplet nucleation and a phase inversion process in a narrow skin layer ($\approx 0.1-1\,\mu m$) during the so-called casting of the membrane [22–27].

Impedance spectroscopy [18, 28, 29] on cellulose acetate and on other desalination membranes supported by steady state [30–32] or initial state [33] EMF characterization of desalination membranes may also reveal the alveolar structure of the active skin layer and the presence of membrane asymmetry. Using a Brüggemann integrated version of the theory of Trukhan [34] for the dielectric response of the Nernst–Planck electro-diffusion in spherical alveoles in nonconducting media, it is possible to estimate the average pore size and the average dielectric permittivity of the pore water and of the continuous polymer phase (with little water). In reference [28] as well as in [29], the average alveolar radius is found to be ≈ 0.7 nm from the increase of the membrane capacitance with external salt concentration. The average relative permittivity of the alveole "water" found varies considerably according to the water content assumed in

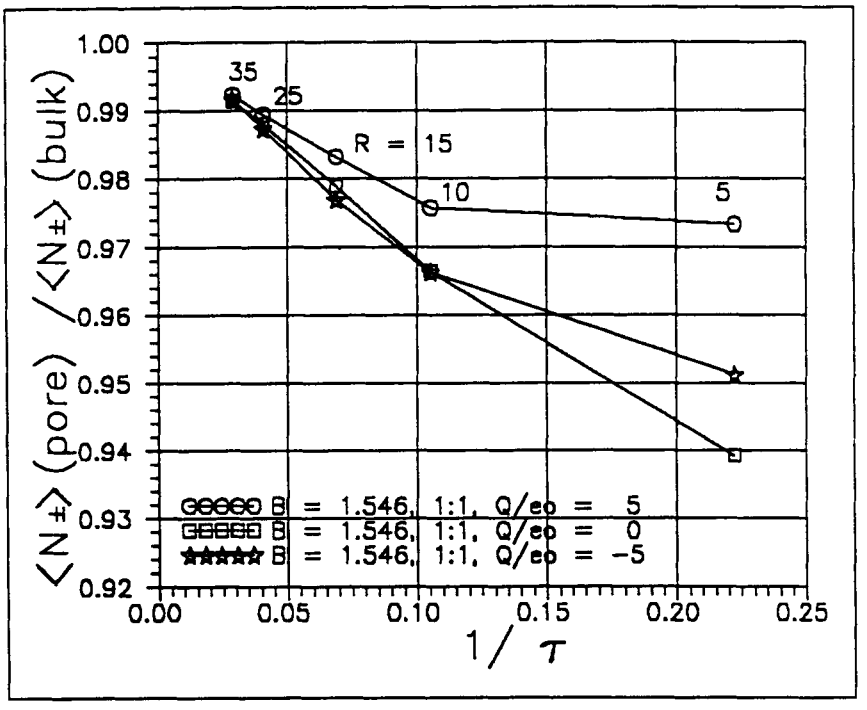

Figure 3b The relative mean occupation numbers for a single pore in equlibrium with the asymmetric 1:1 electrolyte as a function of $1/\tau$. Circles correspond to $Q/e_o = 5$, squares to $Q/e_o = 0$ and stars to $Q/e_o = -5$. The applied potential is $\Delta = 0$, and the pores are not electroneutral. The trend is quite opposite to the one shown in Fig. 3a, which shows the important influence of the Donnan potential in membranes. The decrease in chargeless pores is due to the repulsion of the "mean ion" from the wall (violation of ion cloud symmetry violation). Compared to this trend, we have "electrosorption" in the charged pores, mostly for $Q/e_o = 5$ and small pores (small anions as counterions).

the membrane (difficult to measure). It seems to be 20–30. The relative permittivity of the polymer phase (with little water) is ≈ 15. These values pertain to dense CA membranes or to the active skin layer of asymmetric ultrafiltration CA membranes. For the macroporous support layer, the average alveoles were found to be 200 ± 100 nm from impedance studies, [28] p 379, resulting in an enormous increase in the effective membrane capacitance with salt concentration. The relative permittivity in the alveoles of the support layer is equal to–or close to–the value in bulk water (78.3 at 25°C).

Although the Trukhan theory seems to describe quite well the capacitance part of the impedance of cellulose acetate membranes in salt solutions, there are some conceptual difficulties, however, since the walls are considered impenetrable to ions in the Trukhan theory, but in reality the walls are leaky, and there is certainly a conductivity in the continuous polymer phase, which may be found approximately from Nernst–Planck equations and ideal Donnan distribution theory [28, 29]. A small step in the direction of treating heterogeneous media with leaky walls is the very recent calculation of an

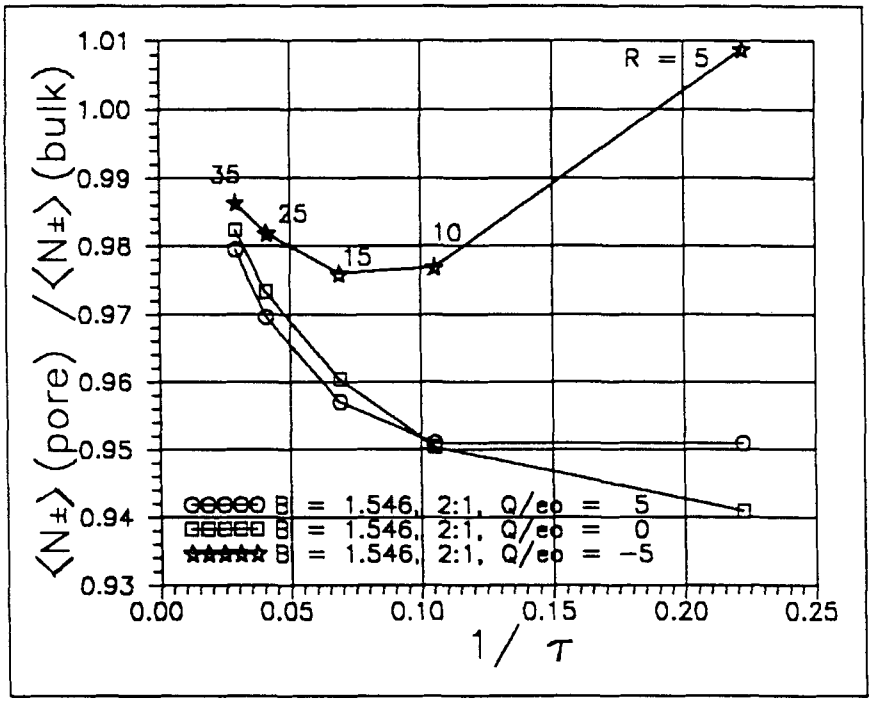

Figure 3c The relative mean occupation numbers for a single pore in equilibrium with the 2:1 electrolyte with $B_r = 1.546$ as a function of $1/\tau$. Circles correspond to $Q/e_o = 5$, squares to $Q/e_o = 0$ and stars to $Q/e_o = -5$. The potential $\Delta = 0$ and the pores are not electroneutral. The "mean ion" is repelled by the wall in chargeless pores, so $\langle N_\pm \rangle / \langle N_\pm \rangle_{bulk}$ decreases with decreasing pore size. Compared to this, there is a weak electrosorption for the smaller pores and $Q/e_o = 5$, and a strong electrosorption in small pores with $Q/e_o = -5$, where the doubly charged cations are counterions to the pore charge.

analytical expression based upon Nernst–Planck equations for the excess impedance of lamellar membranes under very special assumptions [35].

Looking at the equilibrium ion distribution only, the active skin layer of a CA membrane (and in fact in many other desalination membranes as well) may be modelled by means of GCEMC simulations like the present, but to be realistic, the Bjerrum parameter in the alveole should be higher than in the external solution, since the relative permittivity of the water is smaller in the alveole. However, complicated electrostatic interactions with the pore wall should also be accounted for, since the wall material has an even lower relative permittivity. One would expect an *additional* repulsion of ions from a low permittivity wall, than the one found already as a consequence of the asymmetry of the ionic cloud around ions near to the wall, like the negative adsorption of ions near a plane water–air interface found in the theory of Onsager and Samaras [36].

Thus to make even simplified electrochemical and statistical mechanical models of real membranes is a puzzle involving many still unsolved problems, but we have to start

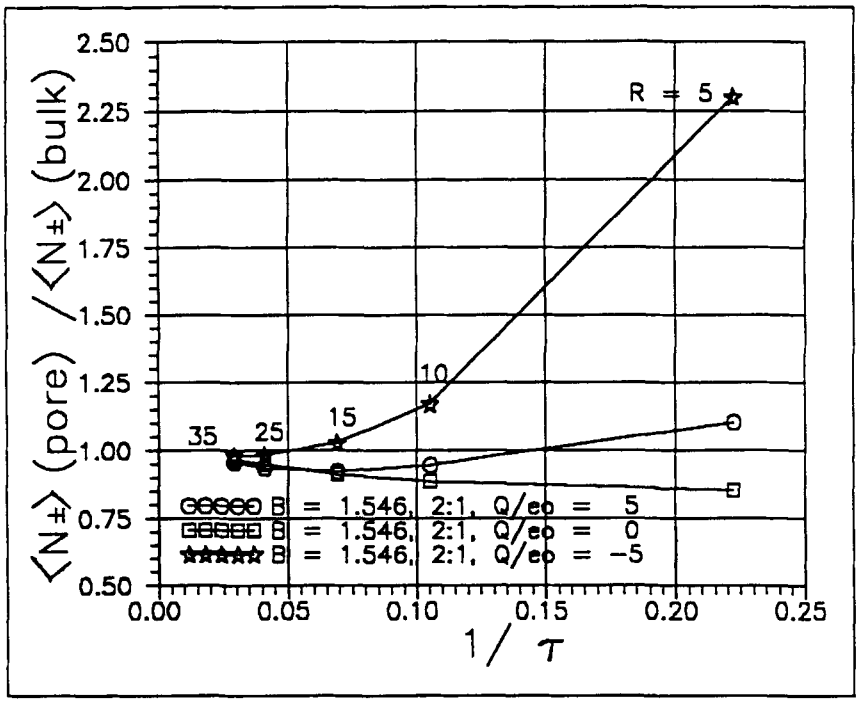

Figure 3d The relative mean occupation numbers for a single pore in equilibrium with the 2:1 electrolyte with $B_r = 3$ as a function of $1/\tau$. Circles correspond to $Q/e_o = 5$, squares to $Q/e_o = 0$ and stars to $Q/e_o = -5$. The potential $\Delta = 0$ and the pores are not electroneutral. Compared to Fig. 3c the decrease in the relative mean occupation numbers with decreasing pore size is much less. This is because a pore with the same R/a is "larger" compared to κ^{-1} for $B_r = 3$ than for $B_r = 1.546$ (at the same electrolyte concentration), since κ^{-1} is smaller. Thus, the repulsion from the wall due to ion cloud symmetry violation is less marked for $B_r = 3$ than for $B_r = 1.546$. Compared to the uncharged pores (squares), the electrosorption for the charged pores is also much stronger than in Fig. 3c, especially when the doubly charged cations are counterions to the pore charge (stars).

somewhere. Here we continue with the GCEMC simulations on primitive, spherical pores (the same permittivity throughout), but with ions of different sizes or absolute value of the ionic charge. Just another small, but necessary, step towards a more fundamental understanding of artificial membranes.

BASIC INPUT/OUTPUT INFORMATION

The model has been explained in the introduction and in previous papers [7, 8, 14], and a detailed description of the design of the Markov process to yield the equilibrium distribution of a (generalized) Grand Canonical Ensemble has been given in reference [14], Appendix A. This description was not restricted to RPM electrolytes, even though all the simulations in the papers [7, 8, 14, 15] were performed using such electrolytes. The procedure has only been generalized slightly in order to be able to sample Helmholtz free energy for the pores, too. This will be described in a later section.

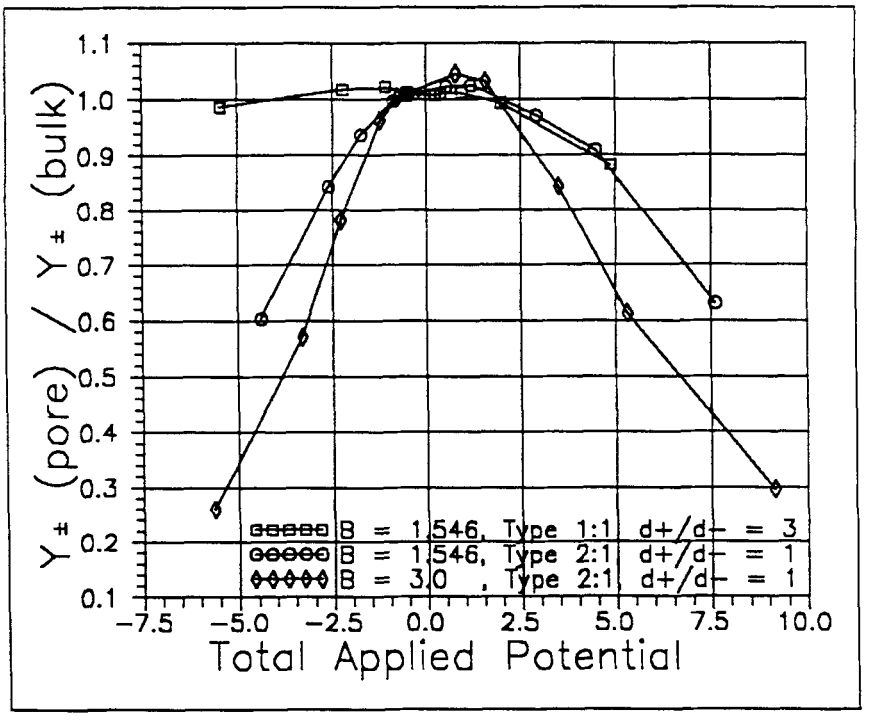

Figure 4 The average mean ionic activity coefficient in the pores relative to the mean ionic activity coefficients in the bulk solutions for the three electrolytes: asymmetric 1:1, $B_r = 1.546$ (squares); 2:1, $B_r = 1.546$ (circles); 2:1, $B_r = 3$ (diamonds) as a function of the dimensionless total applied potential (TAP $= \zeta = \Delta + \eta$). The pores are electroneutral. Bulk properties are almost found in the neighbourhood of TAP = 0. The decrease in the pore mean ionic activity coefficient values with increased absolute values of TAP is clearly asymmetric for positive and negative TAP. Especially the decrease is much more pronounced for the 1:1 electrolyte for positive TAP's, where the small anions are contact adsorbed to the wall. Similarly, the doubly charged cations are contact adsorbed for TAP < 0, especially for $B_r = 3$. The curves are analogous to the electrocapillarity curves of surface tension versus applied potential at an interface between mercury and an electrolyte solution.

The basic input quantities for the bulk electrolyte are given by the

$$\text{electrolyte vector} \equiv (B_r, \rho_s^*, d, z_+, z_-, \nu_+, \nu_-, \mu_+/kT, \mu_-/kT, \mu_{+,\text{HS}}/kT, \mu_{-,\text{HS}}/kT) \quad (1)$$

and the pore properties by the

$$\text{pore vector} \equiv (R/a, Q/e_o, \Delta) \quad (2)$$

with the following definitions:

Reduced Bjerrum parameter:

$$B_r \equiv e_o^2/(4\pi\varepsilon kTa) \quad (3)$$

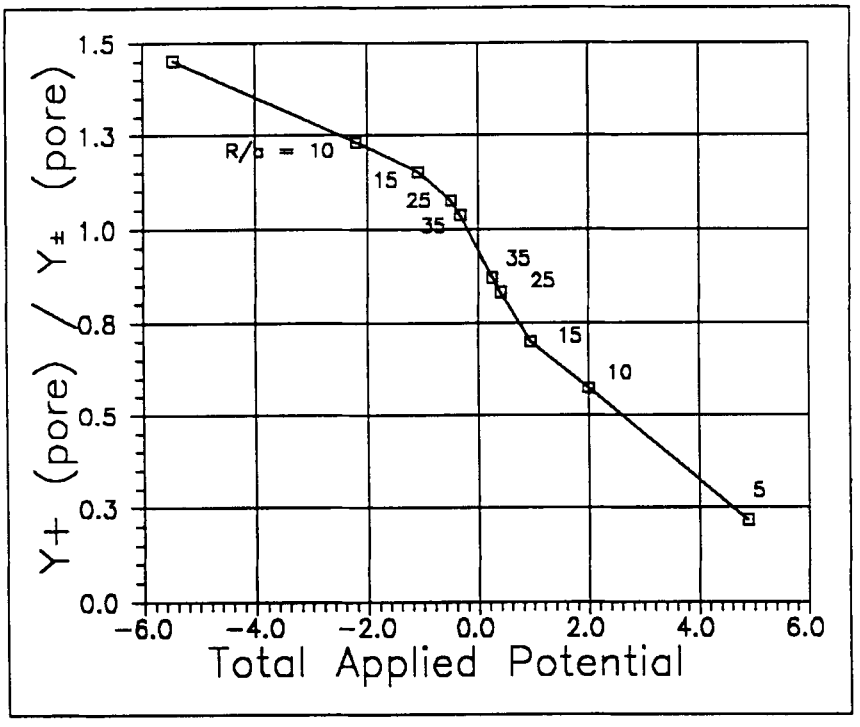

Figure 5 The average single ion activity coefficients for the cation in the pores relative to the average mean ionic activity coefficient in the pore calculated from the simulated Donnan potentials. Asymmetric 1:1 electrolyte, $B_r = 1.546$. Electroneutral pores. The single ion activity coefficients depend strongly on TAP, but at TAP = 0 the ratio is close to unity as in the bulk solution.

(e_o elementary charge, k Boltzmann constant, T absolute temperature)

Mean ion diameter: $$a \equiv (d_+ + d_-)/2 \tag{4}$$

Dimensionless salt density: $$\rho_s^* \equiv \rho_s a^3 \tag{5}$$

Ion diameter ratio: $$d \equiv d_+/d_- \tag{6}$$

Valency of ions (with sign): $$z_+, z_- \tag{7}$$

Stoichiometric coefficients: $$\nu_+, \nu_- \ (\nu \equiv \nu_+ + \nu_-) \tag{8}$$

Dimensionless, bulk excess chemical potential of ionic species i (logarithm of bulk single ion activity coefficient): $$\mu_{i,ex}/kT \equiv \ln y_i \tag{9}$$

Dimensionless, bulk excess chemical potential of ionic species i stripped of charge (logarithm of bulk single ion hard sphere activity coefficient): $\mu_{i,\mathrm{HS}}/kT \equiv \ln y_{i,\mathrm{HS}}$ (10)

Dimensionless radius of alveole: R/a (11)

Dimensionless fixed charge: Q/e_o (12)

Dimensionless additional applied potential in pore relative to the external solution: $\Delta \equiv e_o \Psi_{\mathrm{add}}/kT$ (13)

The hard sphere, excess chemical potentials in the bulk solution, $\mu_{+,\mathrm{HS}}/kT$ and $\mu_{-,\mathrm{HS}}/kT$, were not part of the input in the previous simulations. They are used here for the use in a quantity sampled for the calculation of the electrostatic contribution to the excess Helmholtz free energy. Explanation follows in a later section.

The single ion excess chemical potentials have been found in CEMC simulations by the test particle method of Widom [37, 38] using the correction to electroneutrality derived in reference [17] and the extrapolation methods to the thermodynamic limit described in references [16–20]. The hard sphere contributions are calculated by the generalized Carnahan–Starling formulae of Mansoori et al. [39] as quoted in Ebeling and Scherwinski [40]. Another method is to use MC simulation using again the Widom method (for example with the same programme with $B_r = 0$). The MC and the Mansoori values seem to be very well in accordance up to at least 2 M concentration, see reference [20]. For equal ionic radii, the hard sphere chemical potentials may be calculated by the simple Carnahan–Starling or Percus–Yevick formulae given in reference [20] as Eq. (5) and (6). For the three electrolytes considered:

1:1 electrolyte; $d = 3$; $B_r = 1.546$; $\rho_s^* = 0.0005 (\kappa a = 0.139383)$:

$$\mu_{+,\mathrm{ex}}/kT = -0.09043 \pm 0.00064;\ \mu_{-,\mathrm{ex}}/kT = -0.09234 \pm 0.00043 \tag{14a}$$

(see reference [18], p 180]

$$\mu_{+,\mathrm{HS}}/kT = +0.009179;\ \mu_{-,\mathrm{HS}}/kT = +0.002359 \tag{14b}$$

(Mansoori values)

2:1 electrolyte; $d = 1$; $B_r = 1.546$; $\rho_s^* = 0.00002 (\kappa a = 0.0482837)$:

$$\mu_{2+,\mathrm{ex}}/kT = -0.1380 \pm 0.0002;\ \mu_{-,\mathrm{ex}}/kT = -0.0373 \pm 0.0002 \tag{15a}$$

(see reference [19], Table 11)

$$\mu_{2+,\mathrm{HS}}/kT = \mu_{-,\mathrm{HS}}/kT = +0.0002513 \tag{15b}$$

(CS & PY value)

2:1 electrolyte; $d = 1$; $B_r = 3$; $\rho_s^* = 0.00002 (\kappa a = 0.0672599)$:

$$\mu_{2+,\mathrm{ex}}/kT = -0.390 \pm 0.005; \quad \mu_{-,\mathrm{ex}}/kT = -0.120 \pm 0.003 \tag{16a}$$

(see reference [19], Table 14)

$$\mu_{2+,\mathrm{HS}}/kT = \mu_{-,\mathrm{HS}}/kT = +0.0002513 \tag{16b}$$

(CS & PY value)

Tables 1A–1D show a survey of the simulations performed. The numbering system is continued from the three previous papers [7, 14, 15]. The total number of configurations (= attempts to put and take ions into or from the pore) is 60 millions for all simulations. The pore radii are 5, 10, 15, 25 and 35 mean ionic diameters. The fixed charge—continuously distributed on the pore wall—is $Q/e_o = 5, 0$ and -5. The values of the Δ potential are either zero or the Donnan potential, where the spontaneous electrification of the pore

$$\langle \mathrm{EL} \rangle = Q/e_o + z_+ \langle N_+ \rangle + z_- \langle N_- \rangle \tag{17}$$

is very close to zero. In fact $\langle \mathrm{EL} \rangle / (Q/e_o) < 1\%$ at the stated values of Δ. In order to find the proper value of the Donnan potential, much more runs with different values of Δ around the Donnan potential have been performed than listed in Tables 1A–1D. These runs had less than 60 millions of configurations. The Donnan potentials were determined in analogy with the determinations shown in Figs. 3–5 in reference [14] fitting a least square polynomial to the $\langle \mathrm{EL} \rangle$ vs Δ curves.

In Tables 2A and 2B, the output values of the occupation numbers $\langle N_+ \rangle$ and $\langle N_- \rangle$ are listed in the cases of pore electroneutrality (Donnan conditions) and for $\Delta = 0$, respectively. The values for the $\Delta = 0$ simulations are used for the preparation of Fig. 1, showing plots of the spontaneous electrification of the pores vs $\tau \kappa a$. In Tables 2A and 2B, the values of $\langle N_+^2 \rangle$, $\langle N_-^2 \rangle$ and $\langle N_+ N_- \rangle$ are also listed. From these the variances and the covariance may be calculated. (Also, Kirkwood–Buff cross derivatives of the ionic densities vs the electrochemical potentials may be calculated).

For example, for simulation no. 277 the variance in the sampled N_+ values is

$$\mathrm{VAR}(N_+) = \langle N_+^2 \rangle - \langle N_+ \rangle^2 \approx 0.00926$$

and the variance of the mean value $\mathrm{VAR}(\langle N_+ \rangle)$ is $0.00926/6 \cdot 10^7 \approx 1.54 \cdot 10^{-10}$. Thus, the standard error in $\langle N_+ \rangle$ is ca. $1.2 \cdot 10^{-5}$ and $\langle N_+ \rangle = (9.274 \pm 0.012) \cdot 10^{-3}$. In the same way, the precision of the other values of $\langle N_+ \rangle$ and $\langle N_- \rangle$ may be judged.

Table 1A Survey of simulations performed

Type 1:1, $d_-/d_- = 3$, $B = 1.546$, $\rho_s^* = 5 \times 10^{-4}$, $\mu_-(\text{ex})/kT = -9.043 \times 10^{-2}$, $\mu_-(\text{ex})/kT = -9.234 \times 10^{-2}$, $\mu_+(\text{HS})/kT = 9.179 \times 10^{-3}$, $\mu_-(\text{HS})/kT = 2.359 \times 10^{-3}$

N	Q/e_0	R/a	Δ	*config.* $\times 10^{-6}$
277	5	5	3.332	60
278	5	5	0	60
279	5	10	1.225	60
280	5	10	0	60
281	5	15	0.4360	60
282	5	15	0	60
283	5	25	0.0909	60
284	5	25	0	60
285	5	35	0.01969	60
286	5	35	0	60
287	0	5	0	60
288	0	10	0	60
289	0	15	0	60
290	0	25	0	60
291	0	35	0	60
292	−5	5	−3.910	60
293	−5	5	0	60
294	−5	10	−1.434	60
295	−5	10	0	60
296	−5	15	−0.5680	60
297	−5	15	0	60
298	−5	25	−0.1871	60
299	−5	25	0	60
300	−5	35	−0.1061	60
301	−5	35	0	60

In Tables 3A and 3B, the sampled internal energy $\langle U/kT \rangle$ for the ions in the pores are shown at electroneutrality and at $\Delta = 0$, respectively. The variances $\text{VAR}(U/kT)$ are also shown. The variances of the mean values $\text{VAR}(\langle U/kT \rangle)$ are found by dividing by 60 millions. For example, for simulation no. 277, we have $\langle U/kT \rangle = -4.0155 \pm 0.0001$. The value Ξ_{HS}/Ξ and its variance are also sampled by a special technique to be described later. Ξ and Ξ_{HS} are the Grand Canonical partition functions for the ionic system and the corresponding hard sphere system.

SPONTANEOUS ELECTRIFICATION

When the applied potential Δ is zero, the alveoles are spontaneously electrified at equilibrium as explained in the previous papers. The spontaneous electrification $\langle \text{EL} \rangle$ given by Eq. (17) is calculated from the simulated occupation numbers (listed in Table 2B). In Fig. 1, the values of $\langle \text{EL} \rangle$ are plotted vs the parameter $\tau\kappa a$. The parameter τ is the radius of the accessible spherical volume for the ion in question. Thus, for differently sized ions there are two τs:

$$\tau_+ \equiv (R/a) - (d_+/2a); \quad \tau_- \equiv (R/a) - (d_-/2a) \tag{18}$$

Table 1B Survey of simulations performed

Type 2:1, $d_+/d^- = 1$, $B_r = 1.546$, $\rho_s^* = 2 \times 10^{-5}$, $\mu_+(\text{ex})/kT = -1.38 \times 10^{-1}$, $\mu_-(\text{ex})/kT = -3.73 \times 10^{-2}$, $\mu_+(\text{HS})/kT = 2.513 \times 10^{-4}$, $\mu_-(\text{HS})/kT = 2.513 \times 10^{-4}$

N°	Q/e_o	R/a	Δ	*config.* $\times 10^{-6}$
302	5	5	6.062	60
303	5	5	0	60
304	5	10	3.697	60
305	5	10	0	60
306	5	15	2.398	60
307	5	15	0	60
308	5	25	0.8799	60
309	5	25	0	60
310	5	35	0.3119	60
311	5	35	0	60
312	0	5	0	60
313	0	10	0	60
314	0	15	0	60
315	0	25	0	60
316	0	35	0	60
317	−5	5	−2.864	60
318	−5	5	0	60
319	−5	10	−1.830	60
320	−5	10	0	60
321	−5	15	−1.230	60
322	−5	15	0	60
323	−5	25	−0.5552	60
324	−5	25	0	60
325	−5	35	−0.2668	60
326	−5	35	0	60

These dimensionless radii are used for defining the available volume in the GCEMC programme. In Fig. 1, however, τ is the available radius for a mean ion:

$$\tau \equiv (R/a) - (1/2) \tag{19}$$

A small value of $\tau\kappa a$ means either a small available volume or a small concentration. In both cases the occupation numbers tend to zero, and $\langle \text{EL} \rangle \approx Q/e_o$. This is clearly seen in Fig. 1. A new feature is the fact that for $Q/e_o = 0$ and growing $\tau\kappa a$, the pore no longer remains electroneutral. This is due to the charge or size asymmetry. For the 1:1 electrolyte with $d = 3$ (rectangles), there is a zone near the wall, where only the small anions can stay. Therefore, there is an interfacial layer with a net negative charge. In large pores, the interface is almost planar, and the negative, interfacial charge density becomes approximately constant. The variation in $\langle \text{EL} \rangle$ with $\tau\kappa a$ should then be almost parabolic. The curve in Fig. 1 seems indeed parabolic with a zero slope tangent in $\tau\kappa a = 0$. The two curves for $Q/e_o = 5$ and $Q/e_o = -5$ are not symmetric around $\langle \text{EL} \rangle = 0$ as for RPM electrolytes, but rather around the parabolic curve for $Q/e_o = 0$, which they approach for large $\tau\kappa a$. The pore then approaches electroneutrality in the bulk region, but the excess charge at the interface is the only surviving deviation from electroneutrality.

Table 1C Survey of simulations performed

Type 2:1, $d_+/d_- = 1$, $B_r = 3$, $\rho_s^* = 2 \times 10^{-5}$,
$\mu_+(\text{ex})/kT = -3.90 \times 10^{-1}$, $\mu_-(\text{ex})/kT = -1.20 \times 10^{-1}$,
$\mu_+(\text{HS})/kT = 2.513 \times 10^{-4}$, $\mu_-(\text{HS})/kT = 2.513 \times 10^{-4}$

N°	Q/e_o	R/a	Δ	*config.* $\times 10^{-6}$
327	5	5	6.150	60
328	5	5	0	60
329	5	10	3.808	60
330	5	10	0	60
331	5	15	2.509	60
332	5	15	0	60
333	5	25	0.9800	60
334	5	25	0	60
335	5	35	0.3606	60
336	5	35	0	60
337	0	5	0	60
338	0	10	0	60
339	0	15	0	60
340	0	25	0	60
341	0	35	0	60
342	−5	5	−2.645	60
343	−5	5	0	60
344	−5	10	−1.815	60
345	−5	10	0	60
346	−5	15	−1.274	60
347	−5	15	0	60
348	−5	25	−0.6300	60
349	−5	25	0	60
350	−5	35	−0.3188	60
351	−5	35	0	60

Table 1D Survey of simulations performed

Type 1:1, $d_+/d_- = 3$, $B = 0$, $\rho_s^* = 5 \times 10^{-4}$,
$\mu_+(\text{ex})/kT = 9.179 \times 10^{-3}$, $\mu_-(\text{ex})/kT = 2.359 \times 10^{-3}$,
$\mu_+(\text{HS})/kT = 9.179 \times 10^{-3}$, $\mu_-(\text{HS})/kT = 2.359 \times 10^{-3}$

N°	Q/e_o	R/a	Δ	*config.* $\times 10^{-6}$
352	0	5	0	60
353	0	10	0	60
354	0	15	0	60
355	0	25	0	60
356	0	35	0	60

The 2:1 electrolytes also seem to follow the first part of the parabola for $Q/e_o = 0$. In this case the negative excess charge might be a result of a deficiency of cations near the interface. A doubly charged cation which is not able to form a symmetric ionic cloud near the wall has higher free energy than a singly charged anion. Therefore, the cations will retire more from the wall than the anions.

Table 1E Survey of simulations performed

Type 2:1, $d_+/d_- = 1$, $B = 0$, $\rho_s^* = 2 \times 10^{-5}$, $\mu_+(\text{ex})/kT = 2.513 \times 10^{-4}$, $\mu_-(\text{ex})/kT = 2.513 \times 10^{-4}$, $\mu_+(\text{HS})/kT = 2.513 \times 10^{-4}$, $\mu_-(\text{HS})/kT = 2.513 \times 10^{-4}$

$N°$	Q/e_o	R/a	Δ	*config.* $\times 10^{-6}$
357	0	5	0	60
358	0	10	0	60
359	0	15	0	60
360	0	25	0	60
361	0	35	0	60

Table 2A Occupation numbers and fluctuation quantities at electroneutral conditions

$N°$	$\langle N_+ \rangle$	$\langle N_- \rangle$	$\langle N_+^2 \rangle$	$\langle N_-^2 \rangle$	$\langle N_+ N_- \rangle$
277	9.2735E − 3	5.0056E + 0	9.3463E − 3	2.6890E + 1	5.3110E − 2
279	5.8345E − 1	5.5843E + 0	8.9700E − 1	3.4173E + 1	3.5691E + 0
281	4.2815E + 0	9.2830E + 0	2.1812E + 1	9.1687E + 1	4.1713E + 1
283	2.8063E + 1	3.3065E + 1	8.0550E + 2	1.1124E + 3	9.4086E + 2
285	8.2871E + 1	8.7877E + 1	6.9155E + 3	7.7713E + 3	7.3221E + 3
292	5.0054E + 0	7.4004E − 3	2.6726E + 1	7.4486E − 3	4.2012E − 2
294	5.5646E + 0	5.5865E − 1	3.3856E + 1	8.4776E − 1	3.4011E + 0
296	9.2265E + 0	4.2280E + 0	9.0525E + 1	2.1356E + 1	4.0946E + 1
298	3.3012E + 1	2.8002E + 1	1.1088E + 3	8.0220E + 2	9.3735E + 2
300	8.7770E + 1	8.2757E + 1	7.7525E + 3	6.8971E + 3	7.3034E + 3
302	2.8333E − 7	5.0030E + 0	2.8333E − 7	2.6792E + 1	1.8167E − 6
304	7.9067E − 5	4.9942E + 0	7.9067E − 5	2.7573E + 0	4.7352E − 4
306	2.8975E − 3	5.0048E + 0	2.9035E − 3	2.8179E + 1	1.7058E − 2
308	2.3242E − 1	5.4630E + 0	2.7718E − 1	3.3851E + 1	1.4119E + 0
310	1.9345E + 0	8.8676E + 0	5.2929E + 0	8.5407E + 1	1.8204E + 1
317	2.5013E + 0	1.7969E − 3	6.8419E + 0	1.8000E − 3	5.3372E − 3
319	2.5183E + 0	3.13842E − 2	7.2980E + 0	3.2340E − 2	9.1256E − 2
321	2.5916E + 0	1.7662E − 1	7.9440E + 0	2.0665E − 1	5.1525E − 1
323	3.2612E + 0	1.5210E + 0	1.2465E + 1	3.7657E + 0	5.3546E + 0
325	5.2522E + 0	5.5043E + 0	3.0533E + 1	3.5210E + 1	3.0287E + 1
327	2.7246E − 6	5.0021E + 0	2.7246E − 6	2.6159E + 1	1.8768E − 5
329	2.5690E − 4	5.0052E + 0	2.5690E − 4	2.6916E + 1	1.7086E − 3
331	4.4382E − 3	5.0066E + 0	4.4537E − 3	2.7424E + 1	2.8366E − 2
333	2.2749E − 1	5.4660E + 0	2.6900E − 1	3.3235E + 1	1.4740E + 0
335	1.8652E + 0	8.7311E + 0	4.9127E + 0	8.2472E + 1	1.7790E + 1
342	2.5033E + 0	6.3631E − 3	6.6334E + 0	6.4048E − 3	1.9276E − 2
344	2.5300E + 0	5.6080E − 2	7.0364E + 0	5.9291E − 2	1.7004E − 1
346	2.6150E + 0	2.3103E − 1	7.7137E + 0	2.8409E − 1	7.0956E − 1
348	3.3142E + 0	1.5895E + 0	1.2438E + 1	4.0648E + 0	5.8679E + 0
350	5.2659E + 0	5.5257E + 0	3.0203E + 1	3.5531E + 1	3.1005E + 1

The deviations from electroneutrality for the two 2:1 electrolytes (circles and diamonds) follow almost the same curves as the ones for the 1:1 electolyte, when plotted against $\tau\kappa a$. There are deviations from the pattern for the lower diamond curve ($B_r = 3, 2{:}1$), however. For small values of $\tau\kappa a$, $\langle \text{EL} \rangle$ seems in that case to tend to

Table 2B Occupation numbers and fluctuation quantities at $\Delta = 0$

N	$\langle N_+ \rangle$	$\langle N_- \rangle$	$\langle N_+^2 \rangle$	$\langle N^2 \rangle$	$\langle N_+ N_- \rangle$
278	4.4491 E − 2	7.6841 E − 1	4.5962 E − 2	1.2084 E + 0	4.6433 E − 2
280	1.0573 E + 0	2.8975 E + 0	2.0643 E + 0	1.0454 E + 1	3.4326 E + 0
282	5.0205 E + 0	7.8431 E + 0	2.9090 E + 1	6.6602 E + 1	4.1395 E + 1
284	2.8537 E + 1	3.2530 E + 1	8.3250 E + 2	1.0773 E + 3	9.4137 E + 2
286	8.3051 E + 1	8.7699 E + 1	6.9460 E + 3	7.7405 E + 3	7.3236 E + 3
287	1.5394 E − 1	2.0682 E − 1	1.7046 E − 1	2.3805 E − 1	4.5397 E − 2
288	1.6468 E + 0	1.8250 E + 0	4.0688 E + 0	4.8170 E + 0	3.3893 E + 0
289	6.0969 E + 0	6.4010 E + 0	4.1543 E + 1	4.5526 E + 1	4.1059 E + 1
290	3.0160 E + 1	3.0696 E + 1	9.2810 E + 2	9.6096 E + 2	9.3880 E + 2
291	8.4882 E + 1	8.5641 E + 1	7.2536 E + 3	7.3834 E + 3	7.3094 E + 3
293	5.7787 E − 1	5.6520 E − 2	8.1368 E − 1	5.8991 E − 2	4.4871 E − 2
295	2.6012 E + 0	1.1550 E + 0	8.6475 E + 0	2.3620 E + 0	3.3715 E + 0
297	7.4297 E + 0	5.2317 E + 0	6.0059 E + 1	3.1394 E + 1	4.0873 E + 1
299	3.1902 E + 1	2.8981 E + 1	1.0366 E + 3	8.5829 E + 2	9.3758 E + 2
301	8.6863 E + 1	8.3723 E + 1	7.5939 E + 3	7.0583 E + 3	7.3124 E + 3
303	3.3482 E − 4	6.7613 E − 2	3.3482 E − 4	7.0749 E − 2	5.2567 E − 5
305	1.5389 E − 2	2.8783 E − 1	1.5515 E − 2	3.5740 E − 1	6.5608 E − 3
307	9.7221 E − 2	7.7523 E − 1	1.0356 E − 1	1.3149 E + 0	9.5684 E − 2
309	7.7442 E − 1	2.9674 E + 0	1.2679 E + 0	1.1354 E + 1	2.5648 E + 0
311	2.6807 E + 0	7.5548 E + 0	9.1500 E + 0	6.3197 E + 1	2.1433 E + 1
312	6.7657 E − 3	1.4804 E − 2	6.7777 E − 3	1.4953 E − 2	2.4322 E − 4
313	6.5131 E − 2	1.3977 E − 1	6.7339 E − 2	1.5631 E − 1	1.3522 E − 2
314	2.3684 E − 1	4.9924 E − 1	2.7441 E − 1	7.2474 E − 1	1.4929 E − 1
315	1.1774 E + 0	2.4202 E + 0	2.3236 E + 0	8.0176 E + 0	3.1618 E + 0
316	3.3481 E + 0	6.7898 E + 0	1.3487 E + 1	5.1814 E + 1	2.3996 E + 1
318	1.3276 E − 1	3.7103 E − 3	1.3751 E − 1	3.7218 E − 3	1.0520 E − 3
320	2.6502 E − 1	7.2214 E − 2	3.0292 E − 1	7.6728 E − 2	2.7340 E − 2
322	5.5499 E − 1	3.3408 E − 1	7.6638 E − 1	4.3694 E − 1	2.2880 E − 1
324	1.7526 E + 0	2.0099 E + 0	4.3271 E + 0	5.8913 E + 0	3.8771 E + 0
326	4.1368 E + 0	6.1465 E + 0	1.9698 E + 1	4.3101 E + 1	2.6748 E + 1
328	4.1550 E − 5	2.3991 E − 1	4.1550 E − 5	2.6978 E − 1	4.3983 E − 5
330	5.1242 E − 3	4.9479 E − 1	5.1367 E − 3	6.7515 E − 1	5.5460 E − 3
332	5.0122 E − 2	1.0247 E + 0	5.1645 E − 2	1.9028 E + 0	8.0969 E − 2
334	6.0251 E − 1	3.1959 E + 0	8.8136 E − 1	1.2719 E + 1	2.3204 E + 0
336	2.4256 E + 0	7.6774 E + 0	7.5843 E + 0	6.4875 E + 1	2.0275 E + 1
337	5.6564 E − 3	1.3993 E − 2	5.6611 E − 3	1.4106 E − 2	6.0270 E − 4
338	5.7510 E − 2	1.3397 E − 1	5.8694 E − 2	1.4812 E − 1	1.8587 E − 2
339	2.1812 E − 1	4.8253 E − 1	2.4365 E − 1	6.8632 E − 1	1.6773 E − 1
340	1.1372 E + 0	2.3711 E + 0	2.1303 E + 0	7.7029 E + 0	3.2037 E + 0
341	3.2838 E + 0	6.6972 E + 0	1.2799 E + 1	5.0432 E + 1	2.3783 E + 1
343	7.5330 E − 1	5.3643 E − 3	8.6916 E − 1	5.3934 E − 3	6.8460 E − 3
345	6.1844 E − 1	6.2118 E − 2	7.7468 E − 1	6.5941 E − 2	6.3657 E − 2
347	8.6735 E − 1	2.8991 E − 1	1.3062 E + 0	3.7077 E − 1	3.4749 E − 1
349	2.0208 E + 0	1.8783 E + 0	5.2577 E + 0	5.2831 E + 0	4.3694 E + 0
351	4.3461 E + 0	5.9490 E + 0	2.1181 E + 1	4.0620 E + 1	2.7725 E + 1
352	1.6066 E − 1	2.2440 E − 1	1.8543 E − 1	2.7463 E − 1	3.5721 E − 2
353	1.6591 E + 0	1.9428 E + 0	4.4012 E + 0	5.7180 E + 0	3.2204 E + 0
354	6.0622 E + 0	6.7263 E + 0	4.2774 E + 1	5.1972 E + 1	4.0757 E + 1
355	2.9879 E + 1	3.1755 E + 1	9.2244 E + 2	1.0400 E + 3	9.4870 E + 2
356	8.4103 E + 1	8.7913 E + 1	7.1567 E + 3	7.8165 E + 3	7.3931 E + 3
357	7.6243 E − 3	1.5320 E − 2	7.6808 E − 3	1.5566 E − 2	1.1937 E − 4
358	7.1760 E − 2	1.4370 E − 1	7.6865 E − 2	1.6419 E − 1	1.0289 E − 2
359	2.5494 E − 1	5.1059 E − 1	3.1985 E − 1	7.7102 E − 1	1.3024 E − 1
360	1.2320 E + 0	2.4640 E + 0	2.7489 E + 0	8.5333 E + 0	3.0362 E + 0
361	3.4369 E + 0	6.8782 E + 0	1.5247 E + 1	5.4189 E + 1	2.3637 E + 1

Table 3A Simulated values of thermodynamic quantities (at Donnan potential)

$N°$	$\langle U/kT \rangle$	$VAR(U/kT)$	Ξ_{HS}/Ξ	$VAR(\Xi_{HS}/\Xi)$
277	−4.0155 E + 0	5.1254 E − 1	1.3434 E − 4	1.8532 E − 3
279	−2.06443 E + 0	3.9594 E − 1	9.3459 E − 3	5.2601 E − 1
281	−2.1423 E + 0	9.0172 E − 1	1.5264 E − 1	3.7843 E + 1
283	−5.9654 E + 0	3.9944 E + 0	4.6575 E + 0	3.1619 E + 5
285	−1.5828 E + 1	1.1161 E + 1	3.1038 E + 2	2.8081 E + 9
292	−3.7752 E + 0	4.4343 E − 1	6.0160 E − 5	5.1282 E − 5
294	−1.9628 E + 0	3.9391 E − 1	1.1023 E − 2	9.3534 E + 1
296	−2.0366 E + 0	9.0634 E − 1	1.4931 E − 1	3.0646 E + 2
298	−5.8290 E + 0	4.0590 E + 0	5.1988 E + 0	4.2519 E + 5
300	−1.5655 E + 1	1.1498 E + 0	4.6608 E + 6	2.6863 E + 18
302	−3.8623 E + 0	4.9323 E − 1	6.9002 E − 5	6.7879 E − 5
304	−1.8382 E + 0	2.3203 E − 1	8.5690 E − 4	1.2463 E − 3
306	−1.1882 E + 0	1.4142 E − 1	3.1233 E − 3	1.4144 E − 1
308	−7.4336 E − 1	1.4488 E − 1	5.4884 E − 2	4.8759 E + 0
310	−8.6129 E − 1	4.7465 E − 1	3.7601 E − 1	7.2201 E + 1
317	−5.0614 E + 0	8.3751 E − 1	1.7137 E − 3	3.7420 E − 3
319	−2.3773 E + 0	4.1955 E − 1	1.3511 E − 2	4.9302 E − 2
321	−1.5521 E + 0	3.1540 E − 1	3.6096 E − 2	2.5561 E − 1
323	−1.0928 E + 0	3.8441 E − 1	1.6472 E − 1	5.2709 E + 0
325	−1.2609 E + 0	5.6401 E − 1	4.7062 E − 1	2.4044 E + 1
327	−8.1402 E + 0	1.0021 E + 0	1.0524 E − 6	1.0290 E − 6
329	−3.8765 E + 0	4.9478 E − 1	1.1972 E − 4	1.0365 E − 4
331	−2.5022 E + 0	3.5654 E − 1	8.4035 E − 4	1.3868 E − 1
333	−1.6945 E + 0	1.0403 E + 0	2.5009 E − 2	9.4012 E + 0
335	−2.5498 E + 0	4.3528 E + 0	3.5198 E − 1	2.7864 E + 2
342	−1.0553 E + 1	1.9924 E + 0	7.0528 E − 5	7.0011 E − 5
344	−5.1192 E + 0	1.3134 E + 0	2.7932 E − 3	2.3026 E − 1
346	−3.5105 E + 0	1.5754 E + 0	1.1904 E − 2	5.4530 E − 1
348	−2.89769 E + 0	3.2160 E + 0	8.8807 E − 2	3.4289 E + 1
350	−3.9539 E + 0	6.8682 E + 0	4.6129 E − 1	4.0518 E + 2

a value less in absolute value than 5. The reason is that the doubly charged cations (in a medium of low dielectric permittivity) are *contact adsorbed* to the wall. Thus, the effective absolute value of the wall charge is less than 5. The singly charged anions are apparently not contact adsorbed. In reference [14] we found the same kind of evidence of contact adsorption for a dilute 2:2 electrolyte, when $Q/e_o = 5$ and more pronounced for $Q/e_o = 10$, see reference [14], Fig. 2.

DONNAN POTENTIALS AND AVERAGE PORE ACTIVITIES

The GCEMC Donnan potentials are shown in Fig. 2 as a function of $\tau\kappa a$ for the three kinds of electrolytes and the two fixed charges $Q/e_o = 5$ and -5. The Donnan potentials decrease towards zero for large pore radii or large concentrations. They seem to have vertical asymptotes for $\tau\kappa a \to 0$. Both features are parallelled in the ideal Donnan potentials. The curves for the 1:1 electrolyte are only slightly asymmetric for

Table 3B Simulated values of thermodynamic quantities (at $\Delta = 0$)

N°	$\langle U/kT \rangle$	$VAR(U/kT)$	Ξ_{HS}/Ξ	$VAR(\Xi_{HS}/\Xi)$
278	−1.0633E+0	1.2043E+0	6.0339E−1	7.5311E−1
280	−1.3742E+0	7.5526E−1	5.7596E−1	4.7759E+0
282	−1.9751E+0	1.0314E+0	8.7529E−1	6.1614E+2
284	−5.9589E+0	4.0277E+0	7.6059E+0	2.2508E+5
286	−1.5832E+1	1.1294E+1	5.0349E+2	5.9348E+9
287	−1.1542E−2	1.3738E−2	1.0307E+0	2.2297E−2
288	−2.1625E−1	2.1049E−1	1.2477E+0	1.1642E+0
289	−9.4694E−1	8.0467E−1	1.9400E+0	7.2659E+1
290	−5.2157E+0	3.9707E+0	1.3835E+1	2.1279E+5
291	−1.5217E+1	1.1412E+1	2.3296E+6	7.9234E+17
293	−7.8096E−1	1.0353E+0	7.4786E−1	1.4774E+0
295	−1.1553E+0	8.3095E−1	7.7078E−1	4.5768E+1
297	−1.7828E+0	1.1265E+0	1.1799E+0	3.8410E+2
299	−5.7873E+0	4.0816E+0	8.5803E+0	2.7799E+5
301	−1.5636E+1	1.1380E+1	1.4823E+6	8.0189E+17
303	−1.0298E−1	1.5784E−1	9.5535E−5	2.0693E−1
305	−1.9553E−1	1.7752E−1	9.1167E−1	3.8722E−1
307	−2.9397E−1	2.1552E−1	8.8721E−1	8.3247E−1
309	−4.9294E−1	2.9126E−1	9.3607E−1	5.2517E+0
311	−8.3782E−1	5.4293E−1	1.1677E+0	1.5648E+2
312	−2.1934E−4	3.8079E−4	1.0014E+0	3.5130E−4
313	−4.3365E−3	6.3142E−3	1.0127E+0	8.3823E−3
314	−2.2978E−2	3.0263E−2	1.0419E+0	6.1814E−2
315	−1.6493E−1	1.8808E−1	1.1830E+0	6.9701E−1
316	−5.5435E−1	5.6400E−1	1.5070E+0	2.4043E+1
318	−4.0290E−1	1.1242E+0	8.8691E−1	1.4951E−1
320	−3.5447E−1	5.5011E−1	8.7699E−1	2.3594E−1
322	−4.1537E−1	4.9377E−1	8.7337E−1	3.8600E−1
324	−6.1183E−1	5.6993E−1	9.5368E−1	1.4686E+0
326	−1.0040E+0	8.7065E−1	1.2065E+1	1.3395E+1
328	−7.0978E−1	1.8111E+0	7.9223E−1	3.4401E+0
330	−7.0473E−1	8.5493E−1	7.2723E−1	8.0404E+0
332	−8.9421E−1	7.5592E−1	6.8028E−1	1.0135E+1
334	−1.4324E+0	1.5846E+0	8.0446E−1	9.3953E+1
336	−2.6804E+0	4.7338E+0	1.5009E+1	6.3597E+3
337	−1.7983E−3	7.3430E−3	1.0037E+0	3.2333E−3
338	−2.6097E−2	9.1678E−2	1.0322E+0	7.6989E−2
339	−1.1498E−1	3.5792E−1	1.1082E+0	3.8227E−1
340	−7.1029E−1	1.9370E+0	1.5247E+0	2.0592E+1
341	−2.2093E+0	5.5623E+0	2.8434E+0	8.5904E+2
343	−4.3967E+0	9.2999E+0	3.1115E−3	3.3513E−1
345	−1.7652E+0	3.2100E+0	5.5131E−1	7.2065E−1
347	−1.5579E+0	2.3415E+0	6.0704E−1	2.1047E+0
349	−2.0326E+0	3.3754E+0	8.3695E−1	1.7325E+1
351	−3.4547E+0	6.8674E+0	1.6181E+0	4.3353E+2

the two opposite fixed charges, but for the 2:1 electrolytes the asymmetry is strong at small $\tau\kappa a$. For positive membrane charges, the Donnan potentials here are much greater than those for negative membrane charges. In the latter case, some contact adsorption of the doubly charged cations to the wall charge diminishes the "effective" fixed charge and the Donnan potentials.

This has a parallel in reality, since doubly charged ions like Ba^{2+} or Ca^{2+} do indeed bind to the negative glucuronic acid groups in cellulose acetate membranes. At low ionic strength, the binding is very strong, and it may take up to one month to dissociate the divalent ions from the COO^- groups. The effective fixed charge can even change from negative to positive because of the binding. See references [30–32].

The mean ionic occupation number of the pore is defined by:

$$\langle N_\pm \rangle \equiv [\langle N_+ \rangle^{\nu_+} \langle N_- \rangle^{\nu_-}]^{1/\nu} \tag{20}$$

In this quantity the main influence of the varying total applied potential is removed. Figs. 3a–3d show $\langle N_\pm \rangle_{\text{pore}}/\langle N_\pm \rangle_{\text{bulk}}$ as a function of $1/\tau$. The quantity $\langle N_\pm \rangle_{\text{bulk}}$ is the mean ionic number of ions in a sphere taken out of the bulk solution of radius volume $\text{VOL}_\pm$:

$$\text{VOL}_\pm \equiv [\text{VOL}_+^{\nu_+} \text{VOL}_-^{\nu_-}]^{1/\nu} \tag{21}$$

$$\text{VOL}_+ \equiv (4\pi/3)\tau_+^3; \quad \text{VOL}_- \equiv (4\pi/3)\tau_-^3 \tag{22}$$

$$\langle N_\pm \rangle_{\text{bulk}} \equiv \rho_\pm^* \text{VOL}_\pm \tag{23}$$

$$\rho_\pm^* \equiv [\rho_+^{*\nu_+} \rho_-^{*\nu_-}]^{1/\nu} \tag{24}$$

Why these definitions are reasonable are discussed in the next section.

In Fig. 3a, $\langle N_\pm \rangle_{\text{pore}}/\langle N_\pm \rangle_{\text{bulk}}$ as a function of $1/\tau$ is shown at electroneutral conditions (at the Donnan potential). Each curve represents a given bulk electrolyte and a given pore charge. The smaller the pore and the larger the Bjerrum parameter, the more $\langle N_\pm \rangle_{\text{pore}}/\langle N_\pm \rangle_{\text{bulk}}$ increases relative to unity. The 2:1 electrolytes deviate much more from unity than the 1:1 electrolyte. There is a clear asymmetry between positive and negative pore charges. For the 2:1 electrolytes, the values of $\langle N_\pm \rangle_{\text{pore}}/\langle N_\pm \rangle_{\text{bulk}}$ are higher for $Q/e_o = -5$ than for $Q/e_o = +5$. The additional $\langle N_\pm \rangle_{\text{pore}}$ in the first case is a reflection of the contact adsorption of the doubly charged positive ions. For the 1:1 electrolyte, $\langle N_\pm \rangle_{\text{pore}}/\langle N_\pm \rangle_{\text{bulk}}$ is higher for $Q/e_o = +5$ than for $Q/e_o = -5$. The reason for this difference is that the small anions bind stronger to a positive wall than the large cations to a negative.

In Fig. 3b, $\langle N_\pm \rangle_{\text{pore}}/\langle N_\pm \rangle_{\text{bulk}}$ as a function of $1/\tau$ is shown at the potential $\Delta = 0$ for the 1:1 electrolyte. The picture is quite opposite to the one exhibited in Fig. 3a, which demonstrates the importance of the Donnan potential in membranes. The values of $\langle N_\pm \rangle_{\text{pore}}/\langle N_\pm \rangle_{\text{bulk}}$ *decrease* with the pore size for fixed pore charge. The decrease is the largest for the chargeless pores. This decrease is due to hard sphere exclusion effects. For a pore charge $Q/e_o = -5$, the decrease is slightly less, and the decrease is much less for $Q/e_o = +5$. In the latter case, the reason once more is, that there is a certain adsorption of the small negative anions to the positive wall, which to some degree compensates for the decrease in $\langle N_\pm \rangle_{\text{pore}}$.

Considering a given pore size (τ) in Fig. 3b, one observes an *increase* in $\langle N_\pm \rangle_{\text{pore}}$ with *increasing* absolute value of the pore charge, most markedly for $Q/e_o = +5$, less for $Q/e_o = -5$. This phenomenon was called *electrosorption* in reference [14], since an

increase in $\langle N_{\pm} \rangle_{\text{pore}}$ seems induced by an increase in the absolute value of the total applied potential in the pore (= the constant applied potential inside the pore from Q/e_o + the potential Δ). Figure 3c is parallel to Fig. 3b (with $\Delta = 0$), but the electrolyte is the very dilute 2:1 electrolyte with equal ionic radii and $B_r = 1.546$. The electrosorption is much more marked for $Q/e_o = -5$ than for $Q/e_o = +5$, because of the contact adsorption of doubly charged cations. The tendency is even stronger for a 2:1 electrolyte with $B_r = 3$, Fig. 3d.

It should be noticed, however, that electrosorption as an isolated phenomenon is not directly observable in real membranes with many pores, since a Donnan potential is in that case unavoidable. For example, the curves in Fig. 3a are representative for a Swiss cheese membrane in contact with a 1:1 electrolyte, but not the curves in Fig. 3b. However, both sets of curves demonstrate electrosorption in the sense that $\langle N_{\pm} \rangle_{\text{pore}}$ increases with increased absolute pore charge at constant τ.

The values of $\langle N_{\pm} \rangle_{\text{pore}}/\langle N_{\pm} \rangle_{\text{bulk}}$ are easily translatable to average mean ionic activity coefficients in the pore, since we have (see the next section):

$$y_{\pm}(\text{pore})/y_{\pm}(\text{bulk}) = \langle N_{\pm} \rangle_{\text{bulk}}/\langle N_{\pm} \rangle_{\text{pore}} \tag{25}$$

In Fig. 4, the values of $y_{\pm}(\text{pore})/y_{\pm}(\text{bulk})$ are plotted vs the total applied potential for the three different dilute electrolytes. The values are taken at electroneutrality (at the Donnan potentials). The dimensionless total applied pore potential is given by:

$$\text{TAP} = \zeta = \Delta + \eta = \Delta + (B_r)(Q/e_o)/(R/a) \tag{26}$$

The last term (η) is the dimensionless potential in the ion free pore induced by the pore surface charge.

The asymmetry between positive and negative TAPs is evident in Fig. 4. This asymmetry is due to the charge or size asymmetry. In the neighbourhood of zero TAP, the activity coefficient is maximal. For the 2:1 electrolytes, the lowering in $y_{\pm}(\text{pore})$ is most efficient for negative TAPs. For the 1:1 electrolyte with large cations, positive TAPs lower $y_{\pm}(\text{pore})$ much more than negative.

It should be noticed that the curves are very similar to the classical curves of *electrocapillarity*, i.e., interfacial tensions of a mercury/electrolyte interface as a function of the voltage difference applied between two electrodes. This is not a superficial analogy, since the "adsorption sites" at the interface are analogous to the small pores treated in this study, and the increase in ionic adsorption is linked to the decrease in interfacial tension by the Gibbs adsorption isotherm. The asymmetry of the electrocapillarity curves is explained in similar terms as the asymmetries found here (contact adsorption of small negative ions and/or di- or polyvalent cations).

SINGLE IONIC PORE ACTIVITIES FROM DONNAN POTENTIALS

In this section we generalize the calculation of average single ion pore activities as presented in reference [7], pp 575–576 and in reference [14], pp 137–141 to the case of electrolytes with arbitrary valencies and ion sizes. Let quantities denoted by "p" be pore

quantities and quantities denoted by "b" be bulk quantities. In equilibrium, the electrochemical potentials are equal in the bulk and in the pore for each of the ions:

$$(1/z_+)\ln[\rho_+(p)/\rho_+(b)] + (1/z_+)\ln(y_+(p)/y_+(b)] + \Delta = 0 \tag{27a}$$

$$(1/z_-)\ln[\rho_-(p)/\rho_-(b)] + (1/z_-)\ln[y_-(p)/y_-(b)] + \Delta = 0 \tag{27b}$$

Using that

$$\rho_+(p)/\rho_+(b) = \langle N_+\rangle_p/[\mathrm{VOL}_+\rho_+^*]$$

and the similar equation for the negative ion and subtracting the two Eq. (27a, b), we obtain (taking the exponential at both sides of the equation):

$$[y_+(b)/y_+(p)^{1/z_+}[y_-(p)/y_-(b)]^{1/z_-}$$

$$= [\langle N_+\rangle_p/\{\rho_+^*\,\mathrm{VOL}_+\}]^{1/z_+}[\rho_-^*\,\mathrm{VOL}_-/\langle N_-\rangle_p]^{1/z_-} \tag{28}$$

Using the stoichiometric electroneutrality

$$\nu_+ z_+ + \nu_- z_- = 0 \tag{29}$$

and the definitions (20, 21, 24), we obtain:

$$y_\pm(b)/y_\pm(p) = \langle N_\pm\rangle_p/\{\rho_\pm^*\,\mathrm{VOL}_\pm\} \tag{30}$$

This equation has already been used in the previous section as Eq. (25). Alternatively, we may write Eq. (27a, b) in the form:

$$\langle N_+\rangle_p/\mathrm{VOL}_+ = \rho_+^*\alpha^{-z_+}[y_+(b)/y_+(p)] \tag{31a}$$

$$\langle N_-\rangle_p/\mathrm{VOL}_- = \rho_-^*\alpha^{-z_-}[y_-(b)/y_-(p)] \tag{31b}$$

$$\alpha \equiv \exp(\Delta) \tag{32}$$

Define

$$\delta \equiv z_+\langle N_+\rangle_p + z_-\langle N_-\rangle_p \tag{33}$$

and insert (31a, b):

$$\{-z_-\,n_-\,y_-(b)/y_-(p)\}\alpha^{(z_+ - z_-)} + Q^*\alpha^{z_+} - z_+\,n_+\,y_+(b)/y_+(p) = 0 \tag{34}$$

$$n_+ \equiv [\mathrm{VOL}_+/\mathrm{VOL}_\pm][\rho_+^*(b)/\rho_\pm^*(b)] \tag{35a}$$

$$n_- \equiv [\mathrm{VOL}_-/\mathrm{VOL}_\pm][\rho_-^*(b)/\rho_\pm^*(b)] \tag{35b}$$

$$Q^* \equiv \delta/[\rho_\pm^*(b)\mathrm{VOL}_\pm] \tag{36}$$

For a 1:1 electrolyte, Eq. (34) is an equation of the second degree, for a 2:1 electrolyte Eq. (34) is cubic. Equation (34) is a generalization of Eq. (40) in reference [7] or Eq. (28) in reference [14]. The left-hand side of Eq. (34) is called the *Donnan polynomial*, and it is a generalization of the *ideal Donnan polynomial*, see for example reference [30]. At pore electroneutrality, this polynomial has only one real positive root (α_D) from which the Donnan potential (Δ_D) can be calculated. The Donnan polynomial is central to the calculation of EMF in concentration cells with ion exchange membranes as a separator, see for example, references [18, 30–32], or for the calculation of membrane resistance and capacitance [18, 28, 29].

From Eq. (34), one might calculate the non-ideal Donnan potential using pore electroneutrality: $\delta = -(Q/e_0)$. However, then all the activity coefficients (including average single ion activity coefficients in pores) should be known. This is not the case. The situation is the contrary: The non-ideal GCEMC Donnan potential is known, and one wants to derive information about the single ion activity coefficients in the membrane. We introduce

$$y_{\pm}(p) \equiv [y_{+}(p)^{\nu_{-}} y_{-}(p)^{\nu_{-}}]^{1/\nu} \tag{37}$$

and

$$x \equiv y_{+}(p)/y_{\pm}(p) \tag{38}$$

into Eq. (34) using also the easily derived relation:

$$y_{-}(p)/y_{\pm}(p) = (1/x)^{\nu_{+}/\nu_{-}} \tag{39}$$

The result is:

$$M_1 x^{\nu/\nu_{-}} + M_2 x + M_3 = 0 \tag{40}$$

$$M_1 \equiv -z_{-} n_{-} [y_{\pm}(b)/y_{\pm}(p)] [y_{-}(b)/y_{\pm}(b)] \alpha^{(z_{+} - z_{-})} \tag{41a}$$

$$M_2 \equiv Q^* \alpha^{z_{+}} \tag{41b}$$

$$M_3 = -z_{+} n_{+} [y_{\pm}(b)/y_{\pm}(p)] [y_{+}(b)/y_{\pm}(b)] \tag{41c}$$

Since the value of $y_{\pm}(b)/y_{\pm}(p)$ can be found from Eq. (30), and since $y_{+}(b)/y_{\pm}(b)$ and $y_{-}(b)/y_{\pm}(b)$ are given by the input to the GCEMC simulations, the value of x—and thus the average single ion activities in the pore—can be found as the physically realistic root to Eq. (40). For a 1:1 electrolyte and for a 2:1 electrolyte we have, respectively:

(1:1) $$M_1 x^2 + M_2 x + M_3 = 0 \tag{42}$$

(2:1) $$M_1 x^{3/2} + M_2 x + M_3 = 0 \tag{43}$$

The latter equation is a cubic equation in $\xi \equiv \sqrt{x}$ (missing the term with ξ to the first power). Both cases can be solved analytically. The positive root is chosen for the quadratic equation. For the cubic equation, one finds sometimes a positive discriminant wih one real (and positive) and two complex conjugate roots for ξ. The real, positive solution is then selected, and x calculated. In other cases, one finds a negative discriminant with three real roots given by trigonometric formulae. There is only one positive root for ξ, which is selected, since the square root of x is always positive. The formulae in reference [41] have been used.

In Tables 4–6, the calculated pore average mean ionic and single ion activity coefficients are shown. The ideal Donnan potentials (found from the single real, positive root of the Donnan polynomial with all activity coefficients set to unity and with δ in the Q^* parameter set to $-Q/e_o$) are also listed together with the percent deviation of the GCEMC Donnan potential from the ideal values.

It has been controlled, that the Donnan potentials calculated from the non-ideal Donnan polynomial with the values found for the activity coefficients and with the simulated occupation numbers inserted into the Q^* parameter gives back exactly the values of Δ_{GCEMC}, which were the points of departure.

The deviations from the ideal Donnan potentials are only more than a few per cent in the case of large pores, where the Donnan potential itself is very small and quite insignificant for the membrane properties. This is reassuring, when one considers all the interpretations of membrane EMF, conductivity and capacitance, which have been made using the ideal Donnan potential [27–32].

Figures 5–10 show–for the three kinds of electrolytes–the ratio of the pore average single ionic activity coefficients to the pore average mean ionic activity coefficients as a function of the dimensionless TAP at electroneutrality. This ratio is very sensitive to TAP, most for the 2:1 electrolyte with $B_r = 3$. The ratio is only ≈ 1 at TAP $= 0$.

Figures 11 and 12 show the ratio $y_+(\text{pore})/y_\pm(\text{pore})$ as a function of TAP for the 1:1 electrolyte with $B_r = 1.546$ and $Q/e_o = 5$. The ion diameter ratio $d = 1$ as well as $d = 3$ is shown. The difference is not large between the case $d = 1$ and 3. In Fig. 11, the additional potential is $\Delta = 0$, whereas Δ is the Donnan potential in Fig. 12. The curves are very different in these two cases, but it should be remembered, that it is Fig. 12 which has relevance for any macroscopic portion of a Swiss cheese membrane.

THE ELECTROSTATIC ENERGY, HELMHOLTZ FREE ENERGY AND ENTROPY OF SMALL ALVEOLES

The configurational, electrostatic energy (U) of the ions in the pores has also been sampled for the three electrolytes simultaneously with the occupation numbers. Figure 13 shows the values of $\langle U \rangle / [kT\{\langle N_+ \rangle + \langle N_- \rangle\}]$ vs $1/\tau\kappa a$. The values have been divided by the bulk values E_{ex}/NkT of the excess energy found by extrapolating CEMC simulations for various values of N (total number of ions) to the thermodynamic limit. The extrapolated value of E_{ex}/NkT for the 1:1 electrolyte with $d = 3$ is -0.09711 ± 0.00005, see reference [16], Fig. 12. The extrapolated value of E_{ex}/NkT for the 2:1 electrolyte with $B_r = 1.546$ is -0.0728 ± 0.0003, see reference [19], Fig. 11.

Table 4 $B = 1.546$, 1:1 electrolyte, $\rho_s^* = 5 \times 10^{-4}$, $\mu_+(\text{bulk})/kT = -0.09043$, $\mu_-(\text{bulk})/kT = -0.09234$, $y_+(\text{bulk}) = 0.91354$, $y_-(\text{bulk}) = 0.91180$, $y_\pm(\text{bulk}) = 0.91267$

N	Q/e_o	R/a	Δ_{GCEMC}	Δ_{ideal}	% *dev.*	$y_\pm(pore)$	$x = y_+(p)/y_+(p)$	$y_+(pore)$	$y_-(pore)$
277	5	5	3.332	3.1049	6.81	0.8047	0.7031	0.5658	1.1446
279	5	10	1.225	1.0553	13.9	0.9070	0.8406	0.7624	1.0790
281	5	15	0.4360	0.33060	24.2	0.9239	0.9050	0.8361	1.0209
283	5	25	0.09090	0.05048	44.5	0.9227	0.9622	0.8878	0.9589
285	5	35	0.01969	0.0073273	62.8	0.9197	0.9889	0.9095	0.9300
292	−5	5	−3.910	−3.4386	−12.1	0.9009	1.6253	1.4642	0.5543
294	−5	10	−1.434	−1.2133	−15.4	0.9285	1.2296	1.1417	0.7552
296	−5	15	−0.5680	−0.43406	−23.6	0.9326	1.1355	1.0589	0.8213
298	−5	25	−0.1871	−0.1117	−40.3	0.9244	1.0780	0.9966	0.8575
300	−5	35	−0.1061	−0.050806	−52.1	0.9209	1.0575	0.9739	0.8708

$x = y_+(\text{pore})/y_\pm(\text{pore})$
% *dev.* $= (\Delta_{GCEMC} - \Delta_{ideal})/|\Delta_{GCEMC}|$

Table 5 $B_r = 1.546$, 2:1 electrolyte, $\rho_s^* = 2 \times 10^{-5}$, $\mu_+(\text{bulk})/kT = -0.138$, $\mu_-(\text{bulk})/kT = -0.0373$, $y_+(\text{bulk}) = 0.87110$, $y_-(\text{bulk}) = 0.96348$, $y_\pm = 0.93165$

N	Q/e_o	R/a	Δ_{GCEMC}	Δ_{ideal}	% *dev.*	$y_\pm(p)$	x	$y_+(p)$	$y_-(p)$	*3rd degree equation*
302	5	5	6.062	5.7914	4.45	0.5876	0.2168	0.1274	1.2621	$D > 0$, 1 root
304	5	10	3.697	3.5498	3.99	0.8471	0.5745	0.4866	1.1176	$D > 0$, 1 root
306	5	15	2.398	2.2823	4.82	0.9055	0.7006	0.6344	1.0818	$D > 0$, 1 root
308	5	25	0.8799	0.80211	8.84	0.9554	0.8317	0.7946	1.0476	$D > 0$, 1 root
310	5	35	0.3119	0.26980	13.5	0.9531	0.8710	0.8302	1.0212	$D > 0$, 1 root
317	−5	5	−2.864	−2.8958	1.10	0.5627	1.4521	0.8171	0.4670	$D < 0$, pos. root
319	−5	10	−1.830	−1.7773	−2.88	0.7847	1.2304	0.9655	0.7074	$D < 0$, pos. root
321	−5	15	−1.230	−1.1564	−5.99	0.8735	1.1503	1.0048	0.8145	$D < 0$, pos. root
323	−5	25	−0.5552	−0.48618	−12.4	0.9290	1.0753	0.9990	0.8959	$D < 0$, pos. root
325	−5	35	−0.2668	−0.21397	−19.8	0.9389	1.0362	0.9728	0.9223	$D > 0$, 1 root

$x = y_+(\text{pore})/y_\pm(\text{pore})$
% *dev.* $= (\Delta_{GCEMC} - \Delta_{ideal})/|\Delta_{GCEMC}|$

Table 6 $B_r = 3$, 2:1 electrolyte, $\rho^* = 2 \times 10^{-5}$, $\mu_+(\text{bulk})/kT = -0.390$, $\mu_-(\text{bulk})/kT = -0.120$, $y_+(\text{bulk}) = 0.67706$, $y_-(\text{bulk}) = 0.88692$, $y_\pm = 0.81059$

N°	Q/e_o	R/a	Δ_{GCEMC}	Δ_{ideal}	% *dev.*	$y_\pm(p)$	x	$y_+(p)$	$y_-(p)$	*3rd degree equations*
327	5	5	6.150	5.7914	5.83	0.2405	0.03591	0.008635	1.2689	$D > 0$, 1 root
329	5	10	3.808	3.5498	6.78	0.4969	0.1876	0.09323	1.1470	$D > 0$, 1 root
331	5	15	2.509	2.2823	9.02	0.6833	0.3772	0.2578	1.1123	$D > 0$, 1 root
333	5	25	0.9800	0.80211	18.2	0.8369	0.6171	0.5165	1.0653	$D > 0$, 1 root
335	5	35	0.3606	0.26980	25.2	0.8481	0.7159	0.6071	1.0024	$D > 0$, 1 root
342	−5	5	−2.645	−2.8958	9.48	0.2107	1.9438	0.4095	0.1511	$D < 0$, pos. root
344	−5	10	−1.815	−1.7773	−2.08	0.4629	1.5659	0.7249	0.3700	$D < 0$, pos. root
346	−5	15	−1.274	−1.1564	−9.20	0.6335	1.3341	0.8452	0.5485	$D < 0$, pos. root
348	−5	25	−0.6300	−0.48618	−22.8	0.7807	1.1366	0.8873	0.7323	$D < 0$, pos. root
350	−5	35	−0.3188	−0.21397	−32.8	0.8140	1.0280	0.8368	0.8029	$D > 0$, 1 root

$x = y_+(\text{pore})/y_\pm(\text{pore})$
% $dev. = (\Delta_{GCEMC} - \Delta_{ideal})/|\Delta_{GCEMC}|$

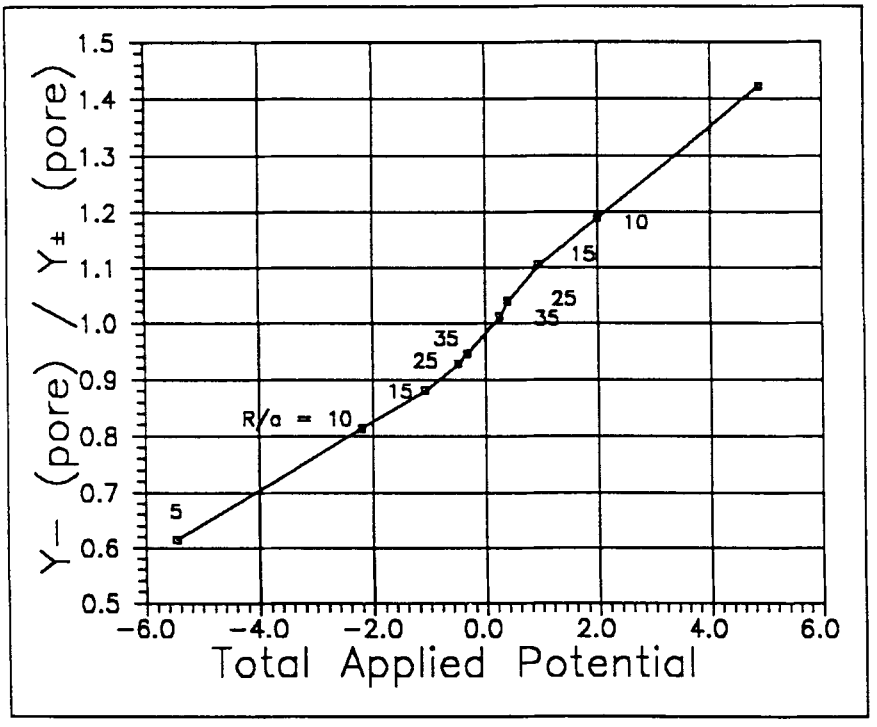

Figure 6 The average single ion activity coefficients for the anion in the pores relative to the average mean ionic activity coefficient in the pore calculated from the simulated Donnan potentials. Asymmetric 1:1 electrolyte, $B_r = 1.546$. Electroneutral pores. The single ion activity coefficients for the anion depend strongly on TAP, but inversely compared to the same quantity for the cation. At TAP = 0 the ratio is close to unity as in the bulk solution.

Finally, for the 2:1 electrolyte with $B_r = 3$, $E_{ex}/NkT = -0.2531 \pm 0.0005$, see reference [19], Table 14.

For $1/\tau\kappa a \to 0$ (large pores), the ratio plotted in Fig. 13 tends to unity as expected. The smaller the pore, the smaller fraction of the electrostatic energy remains. It should be noticed, that in this figure, the energy is solely ion–ion interaction energy, since the pores are without charge. The energy decays most rapidly with decreasing pore size for the 1:1 electrolyte with $d = 3$ and $B = 1.546$ and for the 2:1 electrolyte with $B = 1.546$, and most slowly for the 2:1 electrolyte with $B_r = 3$.

In the case of charged pores the pore energy may be decomposed as

$$U = U_{\text{ion-ion}} + U_{\text{ion-wall charge}} \tag{44}$$

The latter is a contribution from the η potential. There is no contribution from the Δ potential, since we formally place this potential as $-\Delta$ in the external solution

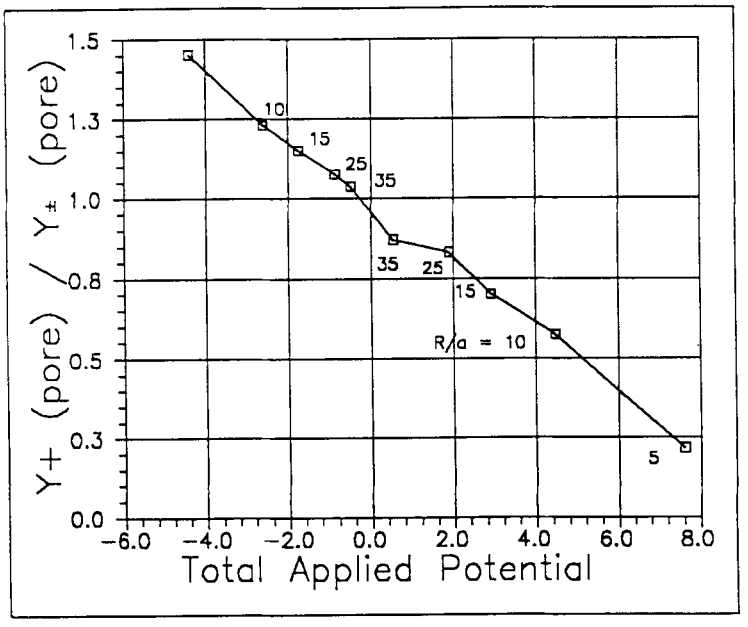

Figure 7 The average single ion activity coefficients for the cation in the pores relative to the average mean ionic activity coefficient in the pore calculated from the simulated Donnan potentials. 2:1 electrolyte, $B_r = 1.546$. Electroneutral pores. The single ion activity coefficients depend strongly on TAP. At TAP = 0 the ratio is close to unity as in the bulk solution.

(affecting the input electrochemical potentials), as was explained in the earlier paper [14].

For the mean energy we have:

$$\langle U/kT \rangle = \langle U_{\text{ion-ion}}/kT \rangle + [z_+ \langle N_+ \rangle + z_- \langle N_- \rangle]\eta \tag{45}$$

In the GCEMC programme $\langle U/kT \rangle$ is calculated, but in Fig. 14 we have plotted the values of $\langle U_{\text{ion-ion}}/kT \rangle / \{\langle N_+ \rangle + \langle N_- \rangle\}$ scaled by the bulk value E_{ex}/NkT vs $1/\tau\kappa a$. The potential in the external solution has been but equal to $-\Delta_{\text{Donnan}}$. We observe that this quantity is $\gg 1$ and negative for small charged pores. Since E_{ex}/NkT is negative itself, the values of $\langle U_{\text{ion-ion}} \rangle$ are positive in contrast to what was found for unchanged pores (Fig. 13, $U = U_{\text{ion-ion}}$). The reason for this is simple: For small pores with high surface charge, the ions with the same charge as the wall charge are almost completely "Donnan excluded". Therefore, there is practically no counterion shielding, and the electrostiatic ion–ion energy has almost only positive contributions. This energy is much greater than the bulk excess energy, or than the excess energy in chargeless pores, where there is counterion shielding. For the same value of $\tau\kappa a$, the above-mentioned effect is the greatest for the 1:1 electrolyte and smallest for the 2:1 electrolyte at $B_r = 3$. The reason is that in the latter case counterions are tightly bound to the doubly charged

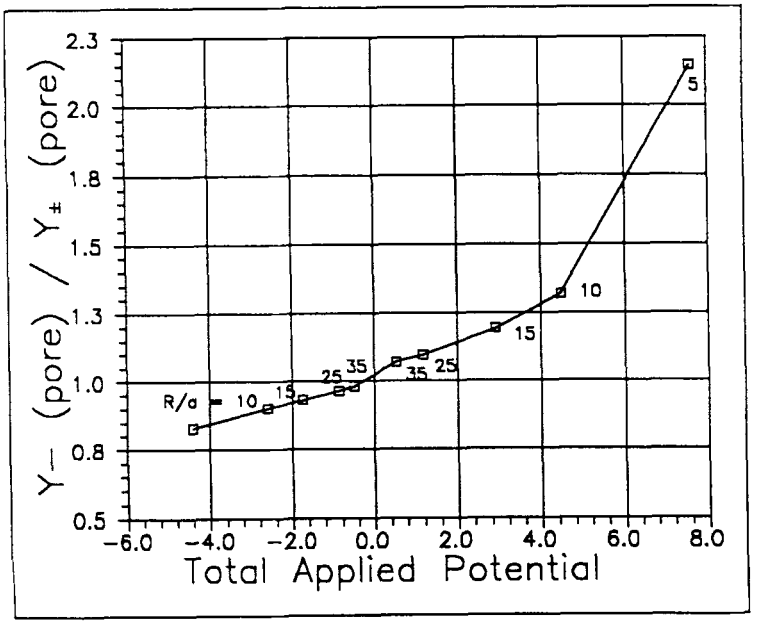

Figure 8 The average single ion activity coefficients for the anion in the pores relative to the average mean ionic activity coefficient in the pore calculated from the simulated Donnan potentials. 2:1 electrolyte, $B_r = 1.546$. Electroneutral pores. The single ion activity coefficients for the anion depend strongly on TAP, but inversely compared to the same quantity for the cation. At TAP = 0 the ratio is close to unity as in the bulk solution.

ions and screen the interactions considerably even in small pores. For $1/\tau\kappa a \to 0$ (large pores), the values of $\langle U_{\text{ion-ion}}/kT\rangle/\{\langle N_+\rangle + \langle N_-\rangle\}$ divided by E_{ex}/NkT tend to unity in all cases as expected, since the influence of the surface charge is then vanishingly small.

In order to be able to calculate the electrostatic Helmholtz free energy for the pore systems, we need to make some derivations. We shall generalize the Monte Carlo method of Salsburg and Chesnut [42–44] along similar lines as done earlier for the CEMC simulations of electrolyte systems [45]. This method has been demonstrated useful for dilute primitive model electrolytes with not too many ions in the simulation cell [16–19, 21].

It is straightforward to show that for the variation in the logarithm of the grand canonical partition function Ξ we have (see, for example, reference [46] p. 54):

$$\begin{aligned} &\mathrm{d}(\ln \Xi + E/kT - (\mu_{+,\mathrm{el}}/kT)\langle N_+\rangle - (\mu_{-,\mathrm{el}}/kT)\langle N_-\rangle) \\ &\quad = \mathrm{d}E/kT + (p/kT)\,dV - (\mu_{+,\mathrm{el}}/kT)\mathrm{d}\langle N_+\rangle - (\mu_{-,\mathrm{el}}/kT)\mathrm{d}\langle N_-\rangle \\ &\quad = \mathrm{d}S/k \end{aligned} \tag{46}$$

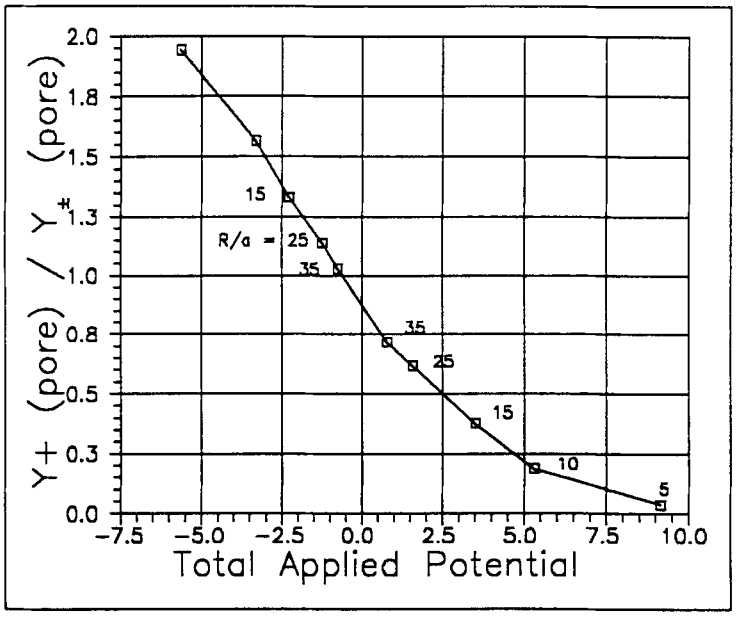

Figure 9 Plot similar to Fig. 7, but for $B_r = 3$. The variation of the ratio is somewhat stronger than for $B_r = 1.546$.

Since the integration constant is zero by the third law of thermodynamics, we have:

$$S/k = \ln \Xi + E/kT - (\mu_{+,\mathrm{el}}/kT)\langle N_+ \rangle - (\mu_{-,\mathrm{el}}/kT)\langle N_- \rangle \tag{47}$$

(S is the entropy, E the internal energy and $\mu_{+,\mathrm{el}}$ is an electrochemical potential). The E and S terms may be combined to the Helmholtz free energy (F):

$$F/kT = -\ln \Xi + (\mu_{+,\mathrm{el}}/kT)\langle N_+ \rangle + (\mu_{-,\mathrm{el}}/kT)\langle N_- \rangle \tag{48}$$

We also write a similar equation for an ideal system of chargeless point particles *with the same number of particles in the pores* (id, A) and subtract the equations (remembering that the bulk dimensionless electric potential is chosen as $-\Delta$)

$$F_{-\mathrm{ex}}/kT = (F - F_{\mathrm{id,A}})/kT = \ln(\Xi_{\mathrm{id,A}}/\Xi) + (\mu_{+,\mathrm{ex}}/kT)\langle N_+ \rangle - (\mu_{-,\mathrm{ex}}/kT)\langle N_- \rangle - \{z_+\langle N_+ \rangle + z_-\langle N_- \rangle\}\Delta \tag{49}$$

with (choosing + or −):

$$\mu_{\pm,\mathrm{ex}}/kT \equiv (\mu_{\pm,\mathrm{bulk}}/kT) - (\mu_{\pm,\mathrm{id,A}}/kT) = \mu_{\pm}(\mathrm{ex,bulk})/kT + \ln\{(\rho^*_{\pm} 4\pi R^3/3)/\langle N_{\pm} \rangle\} \tag{50}$$

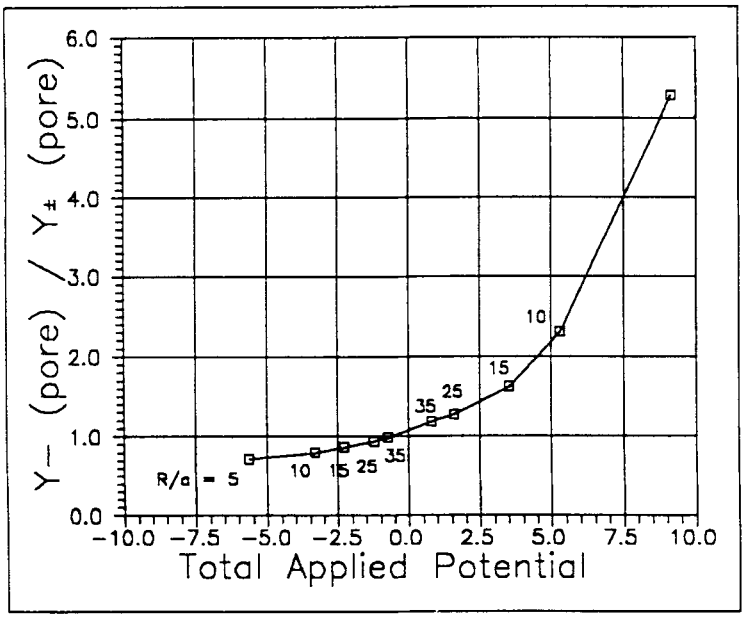

Figure 10 Plot similar to Fig. 8, but for $B_r = 3$. The variation of the ratio is much stronger than for $B_r = 1.546$.

Thus:

$$F_{ex}/kT = \ln(\Xi_{id,A}/\Xi) + [\mu_+(\text{ex, bulk})/kT + \ln\{(\rho_+^* 4\pi R^3/3)/\langle N_+\rangle\}]\langle N_+\rangle + [\mu_-(\text{ex, bulk})/kT + \ln\{(\rho_-^* 4\pi R^3/3)/\langle N_-\rangle\}]\langle N_-\rangle - \{z_+\langle N_+\rangle + z_-\langle N_-\rangle\}\Delta \quad (51)$$

Simulating the corresponding hard sphere system, we obtain an analogous equation:

$$F_{ex,HS}/kT = \ln(\Xi_{id,B}/\Xi_{HS}) + [\mu_+(\text{ex, HS})/kT + \ln\{(\rho_+^* 4\pi R^3/3)/\langle N_+\rangle_{HS}\}]\langle N_+\rangle_{HS} + [\mu_-(\text{ex, HS})/kT + \ln\{(\rho_-^* 4\pi R^3/3)/\langle N_-\rangle_{HS}\}]\langle N_-\rangle_{HS} \quad (52)$$

The grand canonical partition function $\Xi_{id,B}$ is now for an ideal system of chargeless point particles *with the same number of particles in the pores* as for the hard sphere system. Subtracting Eq. (52) from (51) we obain for the excess, *electrostatic* Helmholtz

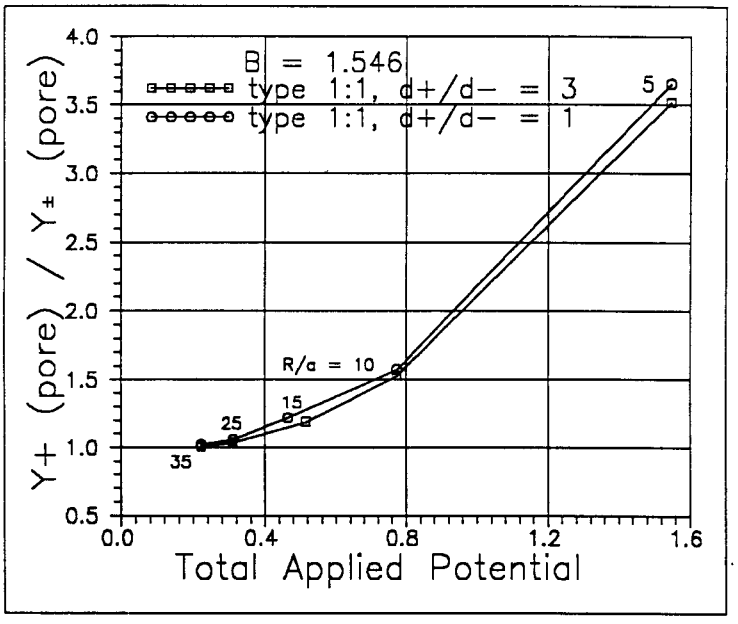

Figure 11 The average single ion activity coefficients for the cation in the pores relative to the average mean ionic activity coefficient in the pore calculated from the GCEMC simulations with $\Delta = 0$ (pores not electroneutral). 1:1 electrolyte, $B_r = 1.546$. Equal radii of cation and anion (circles) and cationic diameter 3 times anionic diameter (squares). Pore charge $Q/e_o = 5$. There is only a slight difference between the symmetric and the asymmetric 1:1 electrolyte. Compared to the right-hand side of Fig. 5 (electroneutral pores, $d = 3$), the dependence of the plotted ratio on TAP is the inverse in the two cases. It is Fig. 5 which is relevant as a model for a real membrane with many pores.

free energy:

$$\begin{aligned}\Delta F_{ex}/kT \equiv F_{ex}/kT - F_{ex,HS}/kT = \ln(\Xi_{HS}/\Xi) + \ln(\Xi_{id,A}/\Xi_{id,B}) \\ + [\mu_+(\text{ex,bulk})/kT + \ln\{(\rho_+^* 4\pi R^3/3)/\langle N_+\rangle\}]\langle N_+\rangle \\ + [\mu_-(\text{ex,bulk})/kT + \ln\{(\rho_-^* 4\pi R^3/3)/\langle N_-\rangle\}]\langle N_-\rangle \\ - [\mu_+(\text{ex,HS})/kT + \ln\{(\rho_+^* 4\pi R^3/3)/\langle N_+\rangle_{HS}\}]\langle N_+\rangle_{HS} \\ - [\mu_-(\text{ex,HS})/kT + \ln\{(\rho_-^* 4\pi R^3/3)/\langle N_-\rangle_{HS}\}]\langle N_-\rangle_{HS} \\ - \{z_+\langle N_+\rangle + z_-\langle N_-\rangle\}\Delta \qquad (53)\end{aligned}$$

Notice that in the present derivation we have avoided to use the usual equation $pV = kT \ln \Xi$ (reference [46], p 58, Table 3.1). This equation is only correct, if the

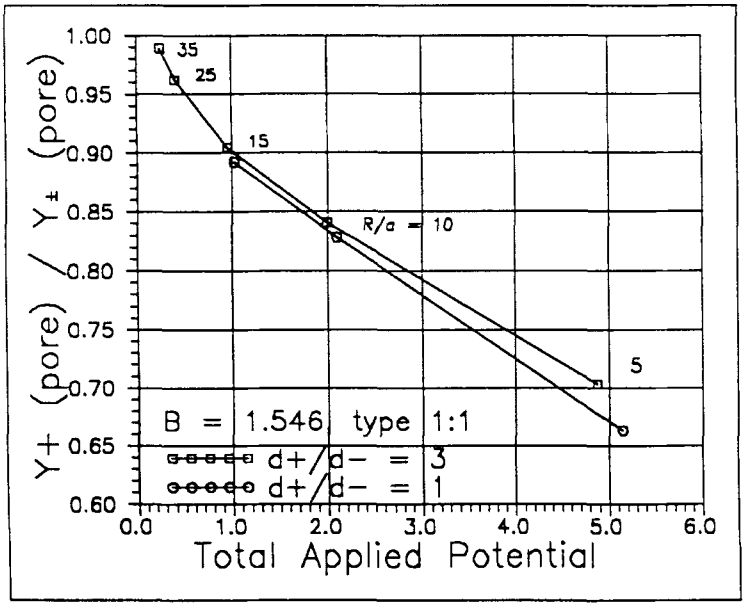

Figure 12 *Plot similar to Fig. 11, but at the Donnan potentials (at electroneutrality). The ratio* $y_+(\text{pore})/y_\pm(\text{pore})$ decreases with increasing TAP in contrast to the case in Fig. 11 (with $\Delta = 0$). But like in Fig. 11, the differences in the ratio between the symmetric and the asymmetric 1:1 electrolyte are not large.

Gibbs–Duhem equation is valid, i.e., when the energy is Euler homogeneous to degree 1. However, here we have also electrostatic effects (Euler degree 2) and surface effects for the small pores. However, Eq. (48) and its consequences, Eq. (49–53), are perfectly general. In calculating the ratio $\ln(\Xi_{\text{id, A}}/\Xi_{\text{id, B}})$ in Eq. (53), however, it is permissible to use $pV = kT \ln \Xi$ no matter how small the pore is, since we now have ideal systems without electrostatic forces and without surface effects destroying the Gibbs–Duhem equations. Since V is the pore volume in both cases, we have:

$$\ln(\Xi_{\text{id, A}}/\Xi_{\text{id, B}}) = (p_A - p_B)\, V_{\text{pore}}/kT = \langle N_+ \rangle + \langle N_- \rangle - \langle N_+ \rangle_{\text{HS}} - \langle N_- \rangle_{\text{HS}} \quad (54)$$

Finally, we demonstrate how to find $\ln(\Xi_{\text{HS}}/\Xi)$ by sampling a special quantity in the GCEMC Markov chain. Let us first be a little more general. The configurational energy is subdivided into a contribution from short range forces (SR) and a long range electric contribution. We then have:

$$U_{\text{el}} = U - U_{\text{SR}} \quad (55)$$

The U_{el} is in fact the energy sampled in our GCEMC programme. (The SR energy is only indirectly felt as rejections of overlapping hard spheres). We now sample the

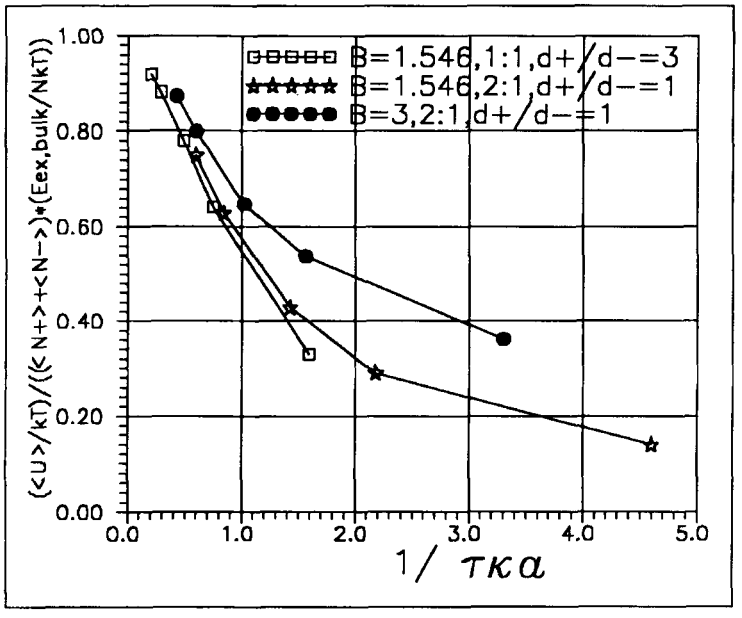

Figure 13 The dimensionless mean excess energy per ion, $\langle U/KT\rangle/\{\langle N_+\rangle + \langle N_-\rangle\}$, in uncharged pores at $\Delta = 0$ from GCEMC simulations divided by the dimensionless excess energy per ion for the bulk electrolytes, E_{ex}/NkT, from CEMC simulations extrapolated to $N \to \infty$. The abscissa is the Debye length (κ^{-1}) divided by the mean available pore radius (τa). The relative excess energies decreases from unity in large pores towards zero in small in proportion to the truncation of the ionic cloud around the ions due to space restrictions. The decrease is most pronounced for the asymmetric 1:1 electrolyte and for the 2:1 electrolyte with $B_r = 1.546$ (squares and stars), least pronounced for the 2:1 electrolyte with $B_r = 3$. In the latter case, there is a certain degree of tight ion pairing contributing to the energy. The ion pairing is much less affected by space restrictions than the diffuse ionic cloud. The values of E_{ex}/NkT are -0.09711 for the asymmetric 1:1 electrolyte, -0.0728 for the 2:1 electrolyte with $B_r = 1.546$ and -0.2531 for the 2:1 electrolyte with $B_r = 3$.

following average:

$$\langle \exp(\{U_{el}/kT\} - \{[\mu_{+,el} - \mu_{+,HS}]/kT\} N_+ - \{[\mu_{-,el} - \mu_{-,HS}]/kT\} N_-)\rangle$$

$$= P/\Xi \tag{56}$$

One obtains

$$P = \sum_N \sum_{\text{states}} \exp(-U_{SR}/kT + [\mu_{+,HS}]/kT\} N_+ + [\mu_{-,HS}]/kT\} N_-) \tag{57}$$

since the "el" quantities cancel for all $\{N_+, N_-\}$ and all energy states. Thus, P is simply the grand canonical partition function for the hard sphere system with "ions" of the same sizes, but without charge. Thus, the quantity sampled yields Ξ_{HS}/Ξ, and by means

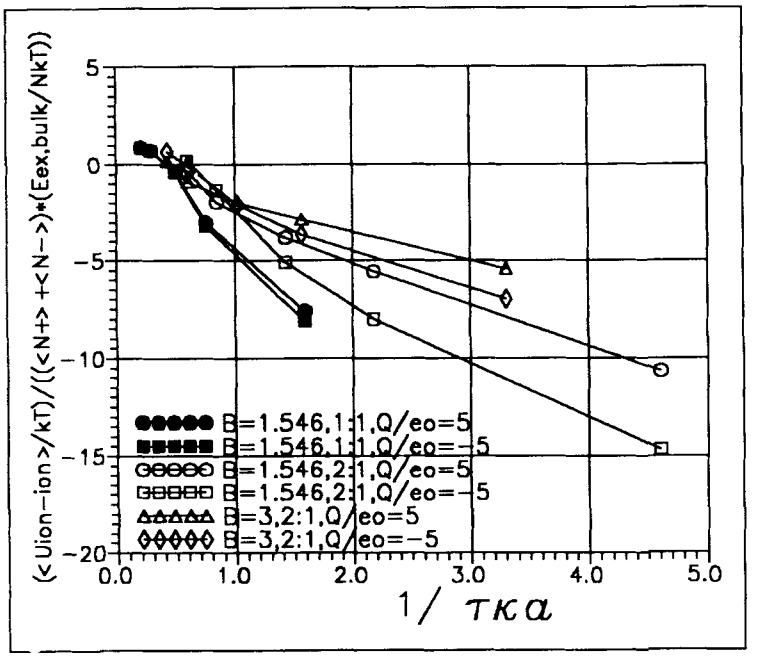

Figure 14 The dimensionless mean ion–ion interaction energy per ion in charged pores at the Donnan potentials divided by the dimensionless excess energy per ion for the bulk electrolytes versus $1/(\tau\kappa a)$. For large pore radii, the relative energies tend to unity, but with decreasing radii, the relative values are increasingly negative. Thus, the ion–ion interaction energies are increasingly positive. This is so because of the Donnan exclusion of ions of the same sign as the pore charge. The number of counterions must balance the pore charge for small, charged pores, and the electrostatic repulsion between the fixed number of counterions is increasing with decreasing pore size. The repulsion is relatively smaller for the 2:1 electrolyte with $B_r = 3$, probably because ion pairing is counterworking total Donnan exclusion of coions.

of Eqs. (53) and (54) we may calculate the excess, electrostatic Helmholtz free energy $\Delta F_{ex}/kT$.

In Fig. 15 we have plotted $(\Delta F_{ex}/kT)/\{\langle N_+\rangle + \langle N_-\rangle\}$ scaled by the extrapolated values of $\Delta F_{ex}/NkT$ from the canonical ensemble calculations (same references as E_{ex}/NkT) as a function of $1/\tau\kappa a$ for the three electrolytes considered. The pores are all without charge. For large pores, all curves tend towards unity (bulk properties). The relative excess Helmholtz free energy first decays with decreasing pore size like the relative excess energy. However, the Helmholtz free energy passes through a minimum and increases slightly again for very small pores. This is true for the two 2:1 electrolytes. It might also be true for the 1:1 electrolyte, but this cannot be seen by the present simulations.

It should be noticed that the value for the 1:1 electrolyte and the large pore radius ($R/a = 35$) has been omitted in Fig. 15, since the value found for Ξ_{Hs}/Ξ was totally off the range of the other values (corresponding to a relative Helmholtz free energy equal to ≈ 2.6). It has been pointed out many times before, that the Salsburg–Chesnut

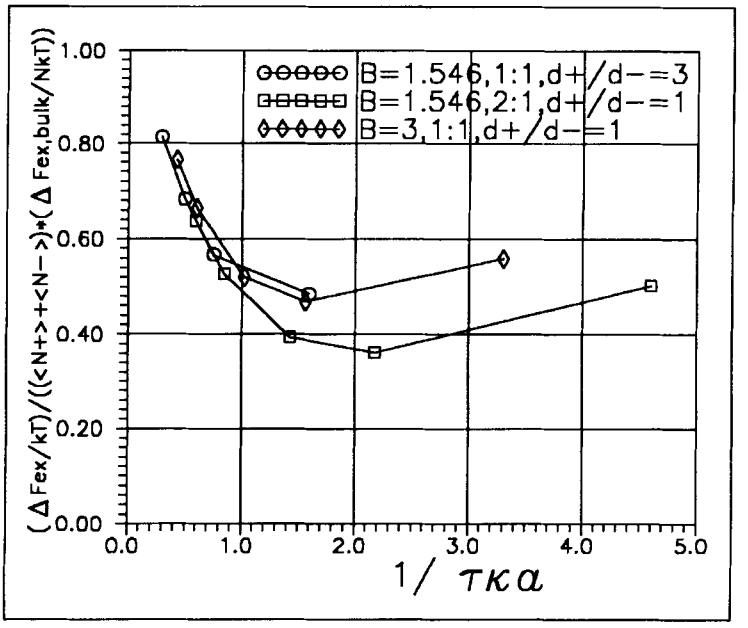

Figure 15 The excess, electrostatic Helmholtz free energy per ion relative to the excess, electrostatic Helmholtz free energy per ion in the bulk electrolytes plotted against $1/(\tau\kappa a)$. The three electrolytes considered are in equilibrium with chargeless pores at $\Delta = 0$. The relative Helmholtz free energies decrease from unity for large pores to smaller values for smaller pores. At least for the 2:1 electrolytes, the relative Helmholtz free energies seem to pass through a minimum and increase slightly again for the smallest pores. The generalized Salsburg–Chesnut simulation method used breaks down at too high interaction energies (large pores, high concentrations). One point for $R/a = 35$ and the 1:1 electrolyte (which is only moderately dilute) has been omitted as totally off the range. The values of the bulk excess quantity $\Delta F_{ex}/NkT$ as extrapolated from CEMC Salsburg–Chesnut simulations are -0.0667 for the asymmetric 1:1 electrolyte, -0.0490 for the 2:1 electrolyte with $B_r = 1.546$ and -0.139 for the 2:1 electrolyte with $B_r = 3$.

procedure (for CEMC) is only successful for dilute systems with not too many interacting particles, i.e., for relatively small interaction energies, if an excessive number of configurations is not to be used [16–19, 21, 45]. Since the present method is a generalization of this procedure to GCEMC, and since the 1:1 electrolyte is only moderately dilute, it is not surprising that the method fails in the greatest pore. The total mean number of cations *plus* anions is ≈ 170. In comparison, for $R/a = 25$, the total number of ions is ≈ 60.

In reference [14] we showed a similar figure (as Fig. 14). However, the quantity plotted there was $\ln\langle\exp(U_{el}/kT)\rangle$ which is equal to $\Delta F_{ex}/kT$, when the average is taken over a canonical ensemble and *not* over a grand canonical ensemble. In that case, only in the limit $1/\tau\kappa a \to 0$ we obtain the (bulk) value of $\Delta F_{ex}/NkT$. With the new kind of sampling used here *all* the points on the curves in Fig. 15 should have physical meaning as the excess Hemholtz free energy over and above the hard sphere free energy.

Figure 16 shows the same relative electrostatic Helmholtz free energy plotted for *charged* pores at electroneutrality. They have the same qualitative features as the curves for $\langle U \rangle / kT$ in charged pores (which we have not plotted). With some scatter all the curves tend to unity (bulk value) for $1/\tau\kappa a \to 0$, and increase to up to 30 times the bulk value for the smallest pores and the highest Bjerrum parameters. Thus the Helmholtz free energies are always negative. For the 1:1 electrolyte, the relative Helmholtz energies increase more for $Q/e_o = 5$ (anions as counterions) as for $Q/e_o = -5$ (cations as counterions). The interpretation is that the small anions have a higher Bjerrum parameter than the mean Bjerrum parameter, whereas the large cations have a lower Bjerrum parameter. For the 2:1 electrolytes, the doubly charged cations have a higher effective Bjerrum parameter than the B_r, and the relative values of the electrostatic Helmholtz free energies for $Q/e_o = -5$ are the higher ones. Thus, in both cases the ion with the higher individual Bjerrum parameter induces the greater increase in the relative Helmholtz free energy, when it is the dominating counterion, at fixed pore size.

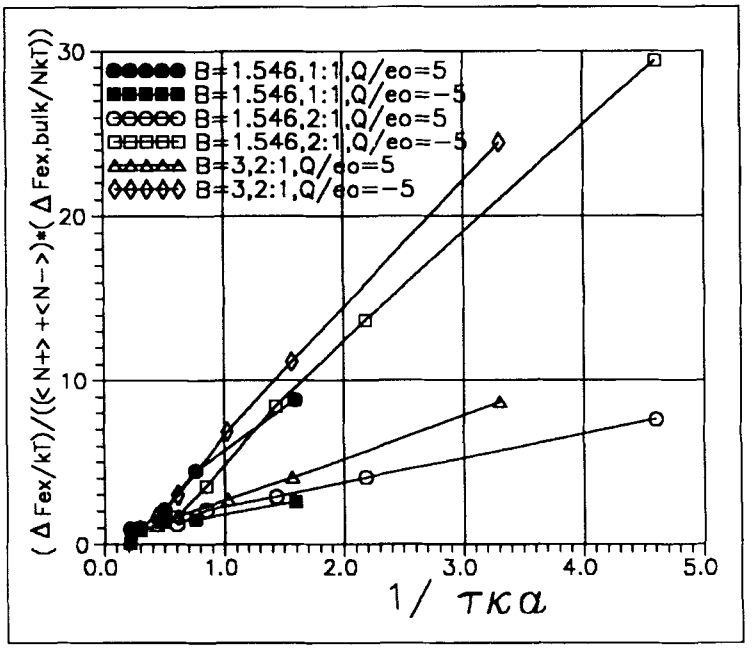

Figure 16 Relative electrostatic Helmholtz free energies per ion in charged pores at the Donnan potential for the three electrolytes considered. For small $1/\tau\kappa a$ the relative Helmholtz free energies are close to unity, but for smaller pores, the relative Helmholz energies are increasing to positive values $\gg 1$. When relative total excess energies (including ion- wall charge interaction) are plotted versus $1/\tau\kappa a$ the curves are qualitatively similar, so in the excess electrostatic Helmholtz free energies the energy effects dominate the entropi effects. This is also apparent in the present plot, where the relative Helmholtz free energies are larger, when doubly charged cations or small anions are counterions to the wall charge.

From the energy and the electrostatic Helmholtz free energy, the excess, electrostatic entropy may be calculated:

$$\Delta S_{ex}/k = \langle U \rangle / kT - \Delta F_{ex}/kT \tag{58}$$

Figure 17 exhibits the relative electrostatic entropies in chargeless pores for the three electrolytes. For $1/\tau\kappa a \to 0$, the bulk limit ($= 1$) is approached. (A completely deviating value for the 1:1 electrolyte and $R/a = 35$ has been omitted, see the above discussion for the relative Helmholtz free energy). For smaller pores, the electrostatic negentropy decreases, and for the smallest pores, the electrostatic entropy may even become positive (the relative entropy negative). We have no ready explanation for that.

For charged pores at electroneutrality (Fig. 18), the relative electrostatic entropies are rising from the bulk limit ($= 1$)—with some scatter for $1/\tau\kappa a \approx 0$—to values up to ≈ 25 for the smallest pores and one of the 2:1 electrolytes. The first thought is that the larger electrostatic negentropy per ion is probably due to the additional structuring induced by the electric double layer in the pore. The increased ordering seems to be most pronounced, when the large cations of the 1:1 electrolyte or the doubly charged

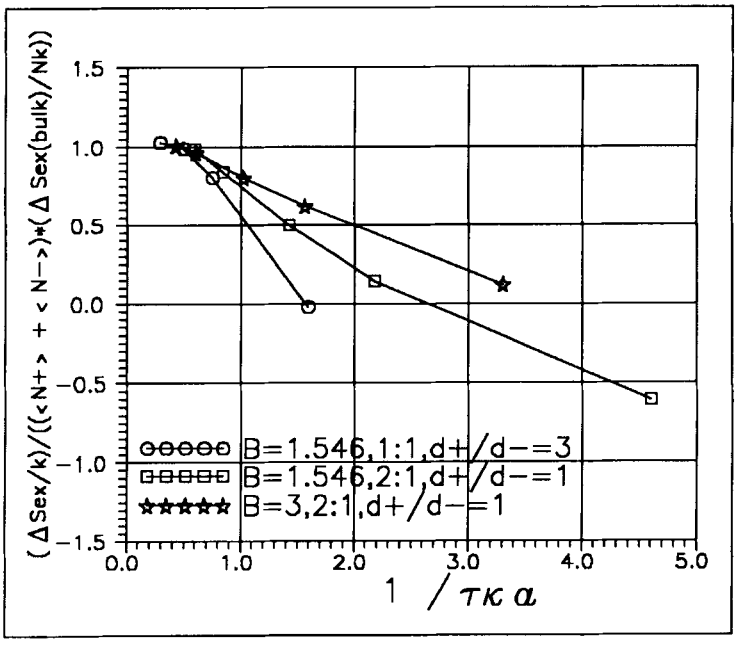

Figure 17 Relative electrostatic entropies in chargeless pores at $\Delta = 0$ as a function of $1/\tau\kappa a$ for the three electrolytes considered. With decreasing pore radius the relative entropies decrease, and they may even become negative, in which case the electrostatic entropy per ion in the pore is positive. The decrease is most pronounced for the asymmetric 1:1 electrolyte, least for the 2:1 electrolyte with $B_r = 3$, most probably because of the ion pairing in the latter case. The bulk, electrostatic excess entropies per ion $\Delta S_{ex}/Nk$ for the three ions are -0.03041 for the asymmetric 1:1 electrolyte, -0.0238 for the 2:1 electrolyte with $B_r = 1.546$, and -0.1141 for the 2:1 electrolyte with $B_r = 3$.

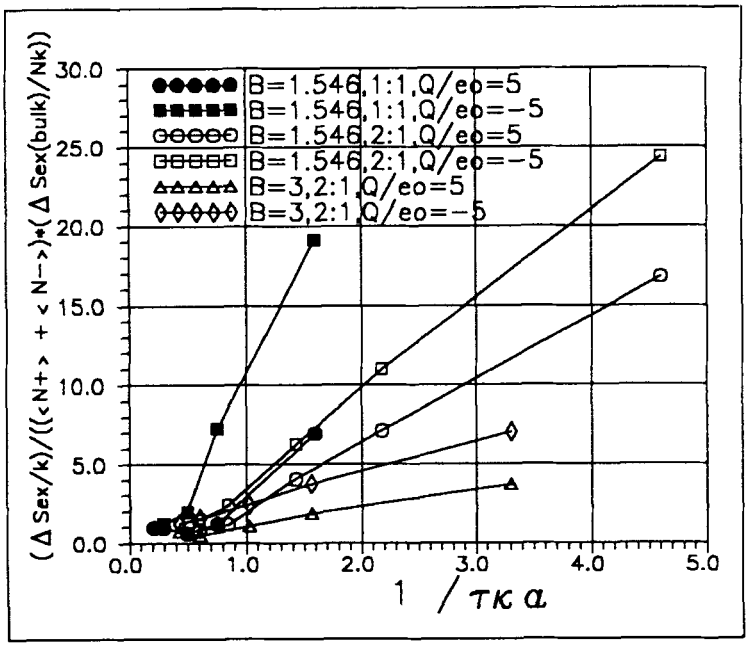

Figure 18 Relative electrostatic entropies per ion in charged pores at the Donnan potential for the three electrolytes considered. For small $1/\tau\kappa a$ the relative entropies are close to unity, but for smaller pores, the relative entropies are increasing to positive values $\gg 1$. A considerable amount of electrostatic ordering seems to be involved, but the pattern is not easy to interpret. See the text for a discussion of some of the effects involved in determining the relative electrostatic entropies.

cations of the 2:1 electrolytes are dominating as counterions. Furthermore, the structuring is the least for the 2:1 electrolyte with $B_r = 3$ and the most for the 1:1 electrolyte with $B_r = 1.546$. This is somewhat contraintuitive. However, we must remember that the quantity plotted is quite a complex one. At the smallest radii, Donnan exclusion tends to be almost complete, so that the number of counterions, and therefore also $\langle N_+ \rangle + \langle N_- \rangle$ approaches $5/|z_{\text{counter}}|$ no matter with which external concentration, the pore is in equilibrium. Furthermore, in that situation the double layer and κ lose their physical significance. Rather, we have $5/|z_{\text{counter}}|$ counterions moving around in a constant external potential. However, the electrostatic repulsion between the ions will favour spread-out positions along the pore-wall of the ions, which increases the negentropy.

DISCUSSION

We have extended the methods from an earlier paper [14] to deal with primitive model electrolytes of different valence types and with different ionic radii in equilibrium with spherical charged pores. It is stressed, that in a "Swiss cheese" membrane with a great many pores, the spontaneous electrification of pores is never seen. The useful values of the activity coefficients in the pores are therefore the ones calculated at the Donnan

potentials (Figs. 4–10, 12). The mean ionic and especially the single ionic activity coefficients are strongly dependent on the "total applied potential" in the pore.

The $y_{\pm}$(pore)/$y_{\pm}$ bulk) vs total applied potential curves resembles electrocapillarity curves, and there are good reasons for this. In the case of a mercury/electrolyte solution interface as well as in the case of small pores, we consider phenomena concerning (electro-)adsorption to interfaces. The adsorption is more dominant at TAPs of opposite charge of the smaller or more highly charged ions, see Fig. 4.

The non-ideal Donnan potentials for the three dilute systems considered mostly deviate less than 10% from the ideal Donnan potentials, when the Donnan potential and the asymmetric ion distribution really matter. Thus, previous EMF and impedance studies of, for example cellulose acetate membranes based on the ideal Donnan distribution are probably quite correct, but the effect of dielectric permittivity differences may play a role (like in the excess impedance at an interface, where it is of fundamental significance, see reference [35]). Figure 2 shows that the precise Donnan potentials at a given radius and salt concentration depend on the salt valency type and the Bjerrum parameter (apart from the pore charge dependence). There is an asymmetry between equal positive and negative pore charges in the case of 2:1 electrolytes or 1:1 electrolytes with different ionic radii. The asymmetry is easily explained in terms of less effective pore charge, when divalent cations or small anions are "contact adsorbed" at the interface. For RPM electrolytes there is no pore charge asymmetry.

When a single pore is in equilibrium with an external solution, the pore is spontaneously electrified (Fig. 1). When the radius of the available pore volume and/or the electrolyte concentration goes to zero, the electrification tends to the effective pore charge, so that strong contact adsorption can be detected. A new feature compared to RPM electrolytes is, that for asymmetric electrolytes, there is a growing electrification with pore radius and/or concentration ($\tau\kappa a$) even for zero pore charge. The growth is approximately parabolic in the radius and reflects that there is an almost constant effective surface charge density due to the difference in the local concentrations of the two ions. The electrifications for sign symmetric pore charges $\pm Q/e_o$ are almost symmetric around the parabolic $Q/e_o = 0$ curve. The electrification for single, noncharged pores means—on the other hand—that there exists nonzero Donnan potentials for Swiss cheese membranes with uncharged alveoles! However, in this study only the Donnan potentials for $Q/e_o = \pm 5$ have been found, not the ones for $Q/e_o = 0$.

We have generalized the Salsburg–Chesnut method for finding Helmholtz free energies by direct MC sampling to GCEMC simulations and primitive electrolytes. The method yields the dimensionless excess, electrostatic Helmholtz free energy $\Delta F_{ex}/kT$ in dilute solutions and not for too large pores. The internal energy of ions in pores $\langle U \rangle/kT$ is also sampled. The dimensionless excess, electrostatic entropy $\Delta S_{ex}/k$ is found as the difference.

It should be noticed, that the generalized Salsburg–Chesnut method requires hard sphere excess chemical potentials as additional simulation input. These may be found from CEMC simulations or from Carnahan–Starling expressions. The simulation output are values of the ratio of the respective grand canonical partition functions: Ξ_{HS}/Ξ. In order to calculate the excess, electrostatic Helmholtz free energy, one needs parallel simulations for similar pore systems with uncharged "electrolytes", since the hard sphere occupation numbers are needed. These simulations have numbers 352–361

(Tables 1D and 1E). We have used the output values given in Table 2B. At the present high or moderate dilutions, these values are within 3 significant digits, the same as the values calculated by the formulae:

$$\langle N_+ \rangle = (4\pi/3)\tau_+^3 \rho_+^*; \quad \langle N_- \rangle = (4\pi/3)\tau_-^3 \rho_-^* \tag{59}$$

In uncharged pores, the values of the internal energy per ion decay from the bulk value at $1/\tau\kappa a = 0$ to zero, when $1/\tau\kappa a \to \infty$ (Fig. 13). The dilute 1:1 electrolyte with unequal ionic radii and $B_r = 1.546$ and the very dilute 2:1 electrolyte with the same reduced Bjerrum parameter seem almost to follow the same curve in the sense that the relative energy per ion scaled by the bulk value is the same function of $1/\tau\nu a$. However, the very dilute 2:1 electrolye with $B_r = 3$ generally has higher relative energies at the same $1/\tau\kappa a$. The reason is that a significant portion of the interaction energy is in the latter case localized in tightly bound counterions rather than in the diffuse Debye–Hückel ionic cloud, so that the truncation of the ionic cloud has not the same effect for the $B_r = 3$ case.

In charged pores, the ion–ion internal energy in the pore as plotted in Fig. 14 is positive for small pores and quite large compared to the absolute value of the bulk internal energy. This is a consequence of the Donnan exclusion of ions of free ions with the same sign as the surface charge. For 2:1 electrolytes, however, a certain amount of ion pairing is found, so that the repulsion energy is less marked, especially for $B_r = 3$.

In uncharged pores, the electrostatic Helmholtz free energy decreases from the bulk value with decreasing pore size, but increases somewhat again for very small pores (Fig. 15)–at least for the dilute 2:1 electrolytes.

In charged pores (at electroneutrality), the relative electrostatic Helmholtz free energies (like the relative electrostatic internal energies including pore charge–ion interactions) are always positive, and the largest increases compared to the bulk values are found, when the ions with the larger effective Bjerrum parameter is the dominating counterion in the pore, see Fig. 16.

In uncharged pores, the relative electrostatic entropies are decreasing from the bulk values with decreasing pore size. The relative entropies may even become negative i.e., excess entropies themselves positive) for the smallest pores (Fig. 17). The decrease in negentropy with decreasing pore size is the least for the 2:1 electrolyte with $B_r = 3$ and the most for the 1:1 electrolyte. The reason is, probably, that for the 1:1 electrolyte the Debye–Hückel ionic cloud is truncated and partially destroyed in small pores, whereas the 2:1 electrolyte with $B_r = 3$ carries a certain percentage of the ions in tightly bound ion pairs, and this structuralization is less influenced by decreasing pore size.

In charged pores (at electroneutrality), the relative electrostatic entropies increase from unity in large pores up to ≈ 25 in small pores. These values seem to be influenced by many factors, so the pattern is less clear (Fig. 18). See the discussion at the end of the previous section.

Acknowledgement

The authors are grateful to Prof., Dr. Vicente Compañ, Dpto. de Física Aplicada y Ciencias Experimentales, Universidad Jaume I, Castellón, Spain, for useful discussions.

References

[1] Y. Zhou and G. Stell, "Fluids inside a pore–an integral-equation approach. I. General formalism and hard spheres inside spherical and slit pores", *Mol. Phys.*, **66**, 767 (1989).

[2] Y. Zhou and G. Stell, "Fluids inside a pore–an integral-equation approach. III. Water-in-oil microemulsions", *Mol. Phys.*, **68**, 1265 (1989).

[3] R. Kjellander and S. Sarman, "Pair correlations of non-uniform hard-sphere fluids in narrow slits and the mechanism of oscillatory solvation forces", *J. Chem. Soc. Faraday Trans.*, **87**, 1869 (1991).

[4] S. J. Zara, D. Nicholson, N. G. Parsonage, and J. Barber, "Mixed valency counterions between charged walls: An investigation using Monte Carlo simulation and comparison with Poisson–Boltzmann theory", *J. Colloid Interface Sci.* **129**, 297 (1989).

[5] V. Vlachy and D. J. Haymet, "Electrolytes in charged micropores", *J. Am. Chem. Soc.*, **111**, 477 (1989).

[6] V. Vlachy and D. J. Haymet, "Salt exclusion from charged and uncharged micropores". *J. Electroanal. Chem.*, **283**, 77 (1990).

[7] T. S. Sørensen and P. Sloth, "Ion and potential distribution in charged and non-charged primitive spherical pores in equilibrium with primitive electrolyte solutions calculated by grand canonical ensemble Monte Carlo simulaton. Comparision with generalized Debye–Hückel and Donnan theory", *J. Chem. Soc. Faraday Trans.*, **88**, 571 (1992).

[8] P. Sloth and T. S. Sørensen, "Hard, charged spheres in spherical pores. Grand canonical ensemble calculations", *J. Chem. Phys.*, **96**, 548 (1992).

[9] F. G. Donnan, "Theorie der Membrangleichgewichte und Membranpotentiale bei Vorhandensein von nicht dialysierenden Elektrolyten. Ein Beitrag zur physikalisch-chemischen Physiologie", *Z. Elektrochemie*, **17**, 572 (1911).

[10] F. G. Donnan,"Die genaue Thermodynamik der Membrangleichgewichte. II" *Z. Physik. Chem. Abt. A.*, **168**, 369 (1934).

[11] T. L. Hill, "On the theory of the Donnan membrane equilibrium" in "Membrane Phenomena", *Discussions of the Faraday Society*, No. 21, 31 (1956).

[12] G. Stell and C. G. Joslin, "The Donnan equilibrium. A theoretical study of the effects of interionic forces", *Biophys. J.* **50**, 855 (1986).

[13] Y. Zhou and G. Stell, "The theory of semipermeable vesicles and membranes: An integral-equation approach. I. General formalism and application to a hard-sphere mixture", *J. Chem. Phys.*, **89**, 7010 (1988).

[14] S. R. Rivera and T. S. Sørensen, "Grand canonical ensemble Monte Carlo simulations of Donnan potentials, nonelectroneutrality, activity coefficients and excess energy in spherical charged or uncharged pores with restricted primitive model electrolytes", *Molecular Simulation*, **13**, 115 (1994).

[15] S. R. Rivera and T. S. Sørensen, "Grand canonical ensemble Monte Carlo simulations of ion distribution functions and of the electric double layer in spherical charged or uncharged pores with restricted primitive model 1:1 electrolytes at moderate concentrations", *Molecular Simulation*, **14**, 35 (1994).

[16] T. S. Sørensen, "How wrong is the Debye–Hückel approximation for dilute primitive model electrolytes with moderate Bjerrum parameter?" *J. Chem. Soc. Faraday Trans.*, **86**, 1815 (1990).

[17] T. S. Sørensen, "Error in the Debye–Hückel approximation for dilute primitive model electrolytes with Bjerrum parameters of 2 and of ca. 6.8 investigated by Monte Carlo methods. Excess energy, Helmholtz free energy, heat capacity and Widom activity coefficients corrected for neutralising background", *J. Chem. Soc. Faraday Trans.*, **87**, 479 (1991).

[18] T. S. Sørensen, "Ions in solution and in weak ion exchange membranes" in *Capillarity Today. Lecture Notes in Physics*, Vol. 386, G. Pétré and A. Sanfeld, eds., Springer-Verlag, Berlin, Heidelberg, New York, London, Paris, Tokyo, Hong Kong, Barcelona, Budapest, 1991 pp 164–221.

[19] T. S. Sørensen, "High precision canonical ensemble Monte Carlo simulations of very dilute primitive z:z and 2:1 electrolytes and of moderately concentrated 1:1 electrolyte mixtures", *Molecular Simulation*, **11**, 1 (1993).

[20] T. S. Sørensen, "A very precise canonical ensemble Monte Carlo determination of thermodynamic properties and of radial distribution functions and electric potentials around ions in a primitive model of 2 M mixtures of KCl and KF at 25°C", *Molecular Simulation*, **14**, 83 (1995).

[21] T. S. Sørensen, "What can be learned from Monte Carlo simulations of simple primitive model electrolyte systems?", in *Trends in Chemical Engineering*, J. Menon, ed., Research Trends, Trivandrum, India, In press 1995, 35 pp.

[22] S. Loeb and S. Sourirajan, "Sea water demineralisation by means of an osmotic membrane", *Adv. Chem. Ser.*, **38**, 117 (1962).

[23] H. Strathman, P. Scheible and R. W. Baker, "A rationale for the prparation of Loeb–Sourirajan type CA membranes", *J. Appl. Polym. Sci.*, **15**, 811 (1971).

[24] U. Merten, ed., *Desalination by Reverse Osmosis*, The M.I.T. Press, Cambridge, Massachusetts and London, England, 1966.
[25] W. Pusch and A. Walch, "Membrane structure and its correlation with membrane permeability; *J. Membr. Sci.*, **10**, 325 (1982).
[26] W. Push and A. Walch, "Synthetic Membranes–preparation, structure and application", *Angew. Chem. Int. Ed. Engl.*, **21**, 660 (1982).
[27] B. Malmgren-Hansen, T. S. Sørensen, and B. Jensen, "Electrochemical characterization of cellulose acetate membranes. 2. Influence of casting conditions and of thermal curing of CA-membranes on the EMF of concentration cells with HCl, LiCl, NaCl and KCl solutions", *J. Non-Equilib. Thermodyn.*, **13**, 193 (1988).
[28] B. Malmgren-Hansen, T. S. Sørensen, and M. Hennenberg, "Electric impedance of cellulose acetate membranes and a composite membrane at different salt concentrations", *J. Colloid Interface Sci.*, **130**, 359 (1989).
[29] I. W. Plesner, B. Malmgren-Hansen, and T. S. Sørensen", Distribution of electrolytes between membraneous and bulk phases, and the dielectric properties of membraneous water, studied by impedance spectroscopy measurements on dense cellulose acetate membranes", *J. Chem. Soc. Faraday Trans.*, **90**, 2381 (1994).
[30] T. S. Sørensen, B. Jensen, and B. Malmgren-Hansen, "Electrochemical characterization of cellulose acetate membranes 1. Influence of hydrogen and calcium ions on the EMF of LiCl concentration cells with a CA-membrane as a separator", *J. Non-Equilib. Thermodyn.*, **13**, 57 (1988).
[31] F. Skácel, B. Malmgren-Hansen, T. S. Sørensen, and B. Jensen, "Electromotive force studies of cellulose acetate membranes. Binding of divalent cations and membrane potentials of KCl-KF mixtures", *J. Chem. Soc. Faraday Trans.*, **86**, 341 (1990).
[32] T. S. Sørensen, B. Jensen, and B. Malmgren-Hansen", Electromotive force and inpedance studies of cellulose acetate membranes: Evidence for two binding sites for divalent cations and for an alveolar structure of the skin layer", *Desalination*, **80**, 293 (1991).
[33] V. Compañ, M. L. López, T. S. Sørensen, and J. Garrido, "Transport numbers in the surface layers of asymmetric membranes from initial time measurements". *J. Physical Chemistry*, **98**, 9013 (1994).
[34] E. M. Trukhan, "Dispersion of the dielectric constant of heterogeneous systems", *Soviet Phys. Solid State*, **4**, 2560 (1963).
[35] T. S. Sørensen, "Nernst-Planckian electrodynamics, the excess interfacial impedance, and the complex permittivity of two semi-infinite phases and of lamellar membranes. The case of identical ionic diffusion coefficients and identical Nernst distribution coefficients", *J. Colloid Interface Sci.*, **168**, 437 (1994).
[36] L. Onsager and N. N. T. Samaras, "The surface tension of Debye-Hückel electrolytes" *J. Chem. Phys.*, **2**, 528 (1934).
[37] B. Widom, "Some topics in the theory of fluids", *J. Chem. Phys.*, **39**, 2808 (1963).
[38] B. Widom, "Potential-distribution theory and the statistical mechanics of fluids", *J. Phys. Chem.*, **86**, 869 (1982).
[39] G. A. Mansoori, N. F. Carnahan, K. E. Starling, and T. W. Leland, "Equilibrium thermodynamic properties of the mixture of hard spheres", *J. Chem. Phys.*, **54**, 1523 (1971).
[40] W. Ebeling and K. Scherwinski, "On the estimation of theoretical individual activity coefficients of electrolytes. I. Hard sphere model", *Z. Physikal. Chem.* (Leipzig), **264**, 1 (1983).
[41] M. R. Spiegel, *Mathematical Handbook of Formulas and Tables*, Schaum's Outline Series, McGraw-Hill, New York, 1968, p 32.
[42] Z. W. Salsburg, J. D. Jacobson, W. Fickett, and W. W. Wood, "Application of the Monte Carlo method to the lattice gas model. I. Two-dimensional triangular lattice", *J. Chem. Phys.*, **30**, 65 (1959).
[43] D. A. Chesnut and Z. W. Salsburg, "Monte Carlo procedure for statistical mechanical calculations in a grand canonical ensemble of lattice systems", *J. Chem. Phys.*, **38**, 2861 (1963).
[44] D. A. Chesnut, "Monte Carlo calculations for the two-dimensional triangular lattice gas: Supercritical region", *J. Chem. Phys.*, **39**, 2081 (1963).
[45] P. Sloth, T. S. Sørensen, and B. Jensen, "Monte Carlo calculations of thermodynamic properties of the restricted, primitive model of electrolytes at extreme dilution using 32, 44, 100, 216, and 512 ions and ca. 10^6 configurations per simulation", *J. Chem. Soc. Faraday Trans.* 2, **83**, 881 (1987).
[46] D. A. McQuarrie, *Statistical Mechanics*, Harper & Row, New York, Evanston, San Francisco, London, 1976, p. 54.